



CZECH TECHNICAL UNIVERSITY IN PRAGUE

**Faculty of Biomedical Engineering
Department of Biomedical Technology**

**Charakterizace výstupní geometrie laserem-buzeného protonového
svazku pro hadronovou terapii**

**Output geometry characterization of the laser-driven ion beam source
for hadron therapy**

Bachelor Thesis

Study Programme: Biomedical and Clinic Technology

Branch of study: Biomedical Technician

Supervisor: Ing. Petr Brůža, Ph. D.

Consultant: Dr. Valentina Scuderi, Ph. D.

Anna Zelená

Kladno, May 2015

Katedra biomedicínské techniky

Akademický rok: 2014/2015

Z a d á n í b a k a l á ř s k é p r á c e

Student: **Anna Zelená**
Obor: Biomedicínský technik
Téma: **Charakterizace výstupní geometrie laserem-buzeného protonového svazku pro hadronovou terapii**
Téma anglicky: Output geometry characterization of the laser-driven ion beam source for hadron therapy

Zásady pro vypracování:

Popište geometrii experimentální sestavy systému pro výběr energie protonů, dříve realizovaného v laboratoři laseru TARANIS, Queens University. Vizualizujte obrazová data 2D dozimetrů - fotoluminiscenčních zobrazovacích desek a vyznačte polohu stopy trasovacího laseru. Na základě obrazových dat fotoluminiscenčních zobrazovacích desek změřte výstupní úhel a divergenci protonového svazku na výstupu systému pro výběr energie protonů. K analýze použijte software ImageJ či Matlab. Diskutujte odchylku výstupního úhlu pro jednotlivé laserové výstřely.

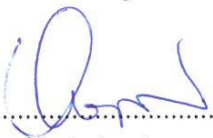
Seznam odborné literatury:

- [1] Scuderi, V., et al., Development of an energy selector system for laser-driven proton beam applications, Nuclear Instruments and Methods in Physics Research Section A: Accelerators, Spectrometers, Detectors and Associated Equipment, ročník 740, číslo 3, 2014, Březen, 87-93 s., doi:10.1016/j.nima.2013.10.037
- [2] Daido H., Nishiuchi, M., Pirozhkov, A.S., Review of laser-driven ion sources and their applications, Reports on Progress in Physics, ročník 75, číslo 5, 2012, Květen, doi:10.1088/0034-4885/75/5/056401
- [3] Hegelich, B.M. et al., Laser acceleration of quasi-monoenergetic MeV ion beams, Nature, ročník 439, číslo 1, 2006, Leden, 441-443 s., doi:10.1038/nature04400

zadání platné do: 11.09.2016

Vedoucí: Ing. Petr Brůža, Ph.D.

Konzultant: Ing. Valentina Scuderi, Ph.D.


.....
vedoucí katedry / pracoviště

l. s.


.....
děkan

V Kladně dne 23.02.2015

Bachelor thesis assignment

Student: **Anna Zelená**

Study branch: Biomedical Technician

Title: **Output geometry characterization of the laser-driven ion beam source for hadron therapy**

Title in Czech: **Charakterizace výstupní geometrie laserem-buzeného protonového svazku pro hadronovou terapii**

Instructions for processing:

Describe the geometry of the experimental energy selector system (ESS) formerly deployed at TARANIS laser facility, Queens University. Visualize the data of 2D dosimeters - photoluminescent imaging plates (IP), and indicate the position of the tracing laser. Using the image data from IPs, measure the angle and divergence of the proton beam at the output of the ESS. The analysis shall be performed in ImageJ or Matlab software. Discuss the deviation of the output angle for different laser shots.


References:

- [1] Scuderi, V., et al., Development of an energy selector system for laser-driven proton beam applications, Nuclear Instruments and Methods in Physics Research Section A: Accelerators, Spectrometers, Detectors and Associated Equipment, vol. 740(3), 2014, March, 87-93 s., doi:10.1016/j.nima.2013.10.037
- [2] Daido H., Nishiuchi, M., Pirozhkov, A.S., Review of laser-driven ion sources and their applications, Reports on Progress in Physics, vol. 75(5), 2012, May, doi:10.1088/0034-4885/75/5/056401
- [3] Hegelich, B.M. et al., Laser acceleration of quasi-monoenergetic MeV ion beams, Nature, vol. 439(1), 2006, January, 441-443 s., doi:10.1038/nature04400

Validity of assignment until date: 11. 9. 2016

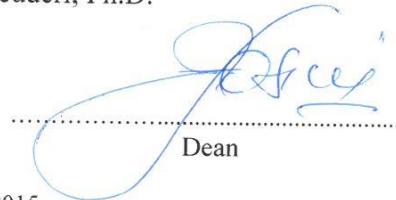
Supervisor of bachelor thesis: Ing. Petr Brůža, Ph.D.

Consultant: Ing. Valentina Scuderi, Ph.D.



Head of Department

L.S.



Dean

In Kladno, 23. 02. 2015

Prohlášení

Prohlašuji, že jsem bakalářskou práci s názvem „Charakterizace výstupní geometrie laserem-buzeného protonového svazku pro hadronovou terapii“ vypracovala samostatně a použila k tomu úplný výčet citací použitých pramenů, které uvádím v seznamu přiloženém k bakalářské práci.

V Kladně dne 21. 5. 2015

.....
Anna Zelená

Acknowledgement

I would like to give my thanks to all who helped me with completing this bachelor thesis, especially to my supervisor Ing. Petr Brůža, Ph. D., to my external consultant Dr. Valentina Scuderi, Ph. D. and to Ing. Martin Přeček Ph. D. for their help and patience with corrections.

Název bakalářské práce:

Charakterizace výstupní geometrie laserem-buzeného protonového svazku pro hadronovou terapii

Abstrakt:

Tato bakalářská práce se zabývá charakterizací laserem-řízených protonových urychlovačů jako budoucí levnější alternativu pro konvenční protonovou léčbu. Nejdůležitější částí, tvořící dopravní systém protonového svazku k pacientovi, je takzvaný systém pro výběr energie, který vybírá pomocí permanentních magnetických dipólů energii potřebnou pro klinickou aplikaci. Hlavním přínosem této práce je geometrický popis takto vzniklého svazku při průchodu a po výstupu ze systému pro selekci energie. Prototyp tohoto systému byl zkonstruován a kalibrován v Laboratoriu Nazionali del Sud v Itálii. Celý systém byl poté testován na laserovém zařízení TARANIS v Belfastu, kde byla i pořízena experimentální data ve spolupráci s panevropským projektem ELI. Data jsem následně podle zadání zpracovala a vyhodnotila. Pro vizualizaci jsem vytvořila v programu *SolidWorks* 3D model systému pro výběr energií s vyznačeným trasovacím laserem a dráhami protonů o různých energiích.

Klíčová slova:

Laserem řízené urychlovače, protonová terapie, systém pro výběr energie, režim TNSA, výstupní úhel, 3D model

Bachelor's Thesis title:

Output geometry characterization of the laser-driven ion beam source for hadron therapy

Abstract:

This bachelor thesis deals with characterization of laser-driven proton accelerators as future cheaper alternative to conventional proton therapy. The most important part of proton beam transport line for the patient is called energy selector system, which chooses through permanent magnetic dipoles the required energy for clinical application. The main goal of this thesis is geometrical description of thus formed beam inside and at the output of energy selector system. A prototype of energy selector system was constructed and calibrated in Laboratori Nazionale del Sud in Italy. The whole system was tested in TARANIS laser facility in Belfast, where the data were taken in cooperation with the pan-European project ELI. According to the assignment of my bachelor thesis I processed and evaluated the data. For visualization I created a 3D model of energy selector system in software SolidWork with alignment laser and proton paths with different energies.

Key words:

Laser acceleration, proton therapy, energy selector system, TNSA regime, output angle, 3D model

Content

List of Figures	9
Introduction	11
1. State of the Art in Hadron Therapy	13
1.1. Biological Effectiveness	15
2. Physical Principles	16
2.1. Lorentz Force.....	16
2.2. Kinetic Energy	17
2.3. Conventional acceleration	19
2.3.1. Cyclotron.....	19
2.3.2. Linear Particle Accelerator.....	21
3. Laser-driven Proton Acceleration	22
3.1. Chirped Pulse Amplification (CPA).....	23
3.2. TARANIS Laser System	25
3.3. TNSA Regime	26
3.4. The Energy Selector System.....	28
4. Experimental Data.....	30
4.1. Imaging Plate	30
4.2. Geometry of Beam Trajectory in ESS	31
4.3. Position of Selection Slit	33
4.4. Output Beam Angle	35
4.4.1. First Shot	35
4.4.2. Second Shot.....	40
5. Conclusion.....	45
References	48

List of Figures

Figure 1: Construction of conventional proton facility with main parts (1 - cyclotron, 2 - electromagnets, 3- gantry) [4]	13
Figure 2: Comparison of the depth–dose relationships for heavy particles (carbon ions and protons) with electrons, X-Rays and gamma rays ^{60}Co . They have a significantly different depth dose curve which shows a narrow Bragg peak at the end for protons and carbon ions. [7]	14
Figure 3: Deflection of the particle for $\mathbf{v} \perp \mathbf{B}$ [9]	16
Figure 4: The purple line shows the classical kinetic energy and the red line the relativistic kinetic energy. [12]	18
Figure 5: Scheme of cyclotron [9].....	20
Figure 6: Scheme of linear accelerator [16]	21
Figure 7: Principal components of CPA laser system (edited from [20]).....	24
Figure 8: Principle of TNSA regime	26
Figure 9: Angular distribution. (The picture is used with permission from presentation “ <i>Transport beamline solutions for laser – accelerated proton beams at ELI-Beamlines</i> ” by A. Tramontana).....	27
Figure 10: Schematic drawing of prototype energy selector system constructed in Catania and tested in TARANIS with dimensions.	29
Figure 11: 3D model of energy selector system made in program SolidWorks	29
Figure 12: 3D model of energy selector system from top view of the particle trajectories at different energies.	29
Figure 13: Magnetic field profiles measured along the radial plane [17]	31
Figure 14: Schematic diagram of the proton beam trajectory inside energy selector system. (r - bending radius, α - bending angle, x_{arc} – transverse displacement, l_{arc} – length of the trajectory, l_{eff} – effective magnetic field length, d is a measure of gap between the first and the second dipole, l_d is length of the proton beam’s path outside the dipole and x_d is deflection of the proton beam in horizontal direction outside the dipole)....	33
Figure 15: The position of selection slit according to required energy of protons	34
Figure 16: 3D model of experimental ESS with IP detector.....	35

Figure 17: A scheme of location of green point laser on a luminescence plate.	36
Figure 18: A picture of the luminescence plate with marked dimensions of the first shot.	36
Figure 19: A) Side view of the ESS output with visualised data from Imaging plate for detector, shot #1, B) The scheme of the vertical deflection of the proton beam from the path of the alignment laser (1 - final collimator, 2 - alignment laser, 3- proton beam, 4 - imaging plate, l_{IP1} – distance from the last collimator to the imaging plate, x_{h1} – height of the proton beam, x_{ver1} – vertical displacement of the proton beam, θ_1 – angle between the alignment laser and the proton beam, δ_1 – divergence of the proton beam).....	38
Figure 20: A) Top view of the ESS output with visualised data from Imaging plate for detector, shot #1, B) The scheme of the horizontal deflection of the proton beam from the alignment laser. (1- final collimator, 2- alignment laser, 3- proton beam, 4- imaging plate, l_{IP1} – distance from last collimator to imaging plate, x_{w1} – width of the proton beam, x_{hor1} – horizontal displacement of proton beam, φ_1 – angle between proton beam and alignment laser, ψ_1 – divergence of proton beam)	39
Figure 21: A scheme of location of green point laser on a luminescence plate for the second shot.	40
Figure 22: A picture of the luminescence plate with marked dimensions of the second shot.	41
Figure 23: A) side view of the ESS output with visualised data from Imaging plate for detector, shot #2, B) The scheme of the vertical deflection proton beam from the alignment laser. (1-final collimator, 2- alignment laser, 3- proton beam, 4- imaging plate, l_{IP2} – distance from last collimator to imaging plate, x_{h2} – height of the proton beam, x_{ver2} – vertical displacement of proton beam, θ_2 – angle between alignment laser and proton beam, δ_2 – divergence of proton beam).....	42
Figure 24: A) Top view of the ESS output with visualised data from Imaging plate for detector, shot #2 B) The scheme of the horizontal deflection proton beam from trace laser (1-final collimator, 2- alignment laser, 3- proton beam, 4- imaging plate, l_{IP2} – distance from last collimator to imaging plate, x_{w2} – width of the proton beam, x_{hor2} – horizontal displacement of proton beam, φ_2 – angle between proton beam and alignment laser, ψ_2 – divergence of proton beam)	44

Introduction

Particle accelerators are used today in many fields of science. They became very important in medical field, especially in cancer treatment. Treatment of cancer is and always will be a topical issue. Currently there are multiple treatment options, the most important being surgery, chemotherapy, and radiation therapy.

A big advantage of radiotherapy is in the possibility of localization of deep-seated local tumours and sparing most of the healthy tissue around the malignant tissue. Currently, radiation treatment experiences a huge progress in proton therapy, which is more precise in dose delivery into tumour. [1] The wider application of this method is limited by the high costs of procedure and construction of conventional accelerators. Therefore, prospectively new methods of proton acceleration with laser that could be used for hadron therapy are being developed [1] and a preliminary characterization of the related proton beam handling is also the main scope of this thesis.

Conventional methods used for acceleration of charged particles are realised by mainly large cyclotrons and synchrotrons whose construction and beam delivery system require a dedicated facility. The complexity of such system also drives the high cost of conventional proton therapy infrastructure and maintenance costs, as well as the cost of individual procedures. A relevant option to the conventional proton therapy is laser-driven proton acceleration technique, which have the potential to scale down the complexity and costs of future proton therapy.

First successes in the progression of laser-driven acceleration have already been achieved. Currently, experiments employing the TNSA regime (target normal sheet acceleration) are being pursued. However, so far, the accelerated particles have a wide range of energy, while for multidisciplinary and, particular, medical application it is necessary to select only one required energy (achieve highly monochromatic beam). A prototype of an energy selector system (ESS) has been constructed to achieve a satisfactory energy distribution of proton energy. The ESS prototype was realized and calibrated at the INFN Laboratory Nazionali del Sud in Catania, Italy in the energy range between 4 and 12 MeV using a conventional accelerated proton beam. The ESS prototype

was characterized for the time using the laser-driven proton beam available at the laser laboratory TARANIS at Queens University Belfast, UK.

The goal of this bachelor thesis was to describe the geometry of the ESS and to measure the output angle and divergence of the proton beam at the exit point. For this purpose the image processing software *ImageJ* was used. The data of 2D dosimeters - photoluminescence imaging plates were analysed and visualized, and mark the position of the trace given by alignment laser. Towards the end, the deviation of the output angle for two laser shots is discussed, working with mathematic model of the proton path inside the ESS and the location of selection slit for required energy. This mathematical model has been realised using the *Matlab* software and used for the construction of a 3D model in the *SolidWorks* software.

The primary interest was to find simple laws, which would allow the investigation and measurement parameters of the ion beams, e.g. maximum ion energy or shape of the energy spectrum. Laser-driven acceleration is a very complex process involving many physical phenomena. The most important ones are ionization, preplasma formation, absorption of the main energy of pulse to electrons, laser driven evolution of plasma and ion propagation after and during the acceleration. [1]

Because of limited possibilities of detection, it may be difficult to determine a dominant mechanism of acceleration. Parameters characterizing the plasma, such as electron density and electron temperature, cannot be exactly determined beforehand and can only be estimated with up to a certain degree of reliability. Due to these difficulties, successive generation of proton beams shows poor reproducibility.[1]

1. State of the Art in Hadron Therapy

Radiation therapy is based on the idea of selective cell destruction. It uses ionizing radiation that can kill cells or change genes so the cells stop growing. During the conventional treatment a photon beam is applied into a tumor, which also affects the healthy tissues behind it, especially the very sensitive tissues like brain, lungs or spinal cord are threatened. This problem can be partly solved by proton therapy, because of difference in the depth-dose distribution.

Proton therapy has proven to be effective and advantageous in number of tumor treatments, employing protons or heavy ions from synchrotrons, cyclotrons or linear particle accelerators. During proton therapy it is necessary to produce particles with energy about 60-250 MeV, which are able to deliver doses at clinically relevant depths (from few cm to 25 cm). [2] Proton cyclotrons for energies up to 235 MeV are approximately 4 meters in diameter, while synchrotrons of capable of accelerating protons to 250 MeV are even larger, around 10 meters in diameter. [3] Large and heavy gantries are used to transport the beam to the patient (see in Figure 1). The support structures must be able to rotate the whole gantry system around the patient with high precision. For this reason it is necessary to build a special building, where these accelerators and gantries placed.

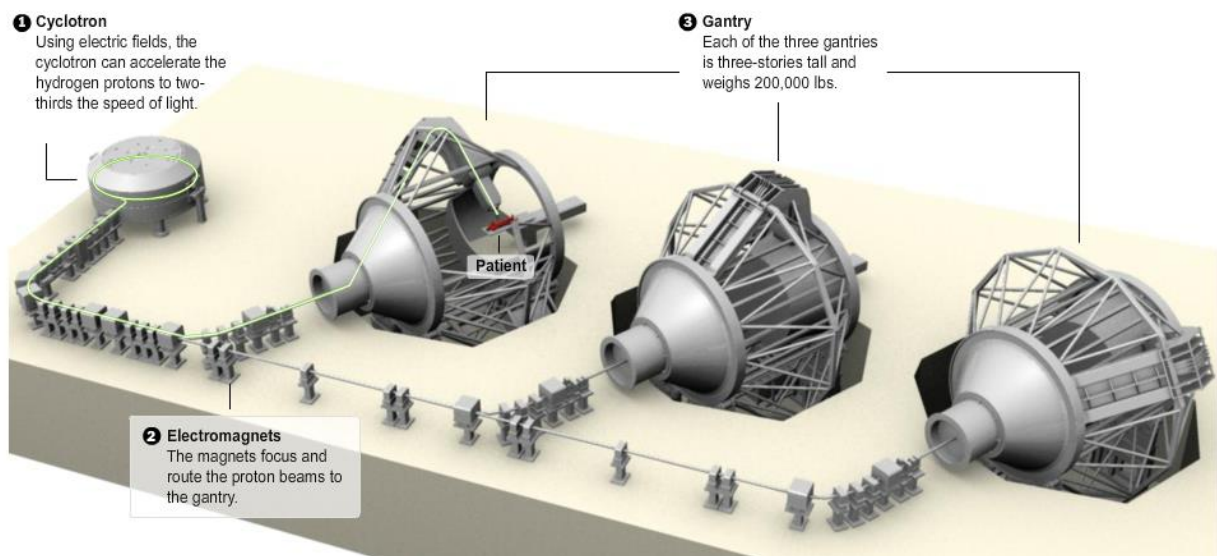


Figure 1: Construction of conventional proton facility with main parts (1 - cyclotron, 2 - electromagnets, 3- gantry) [4]

Hadron therapy is an external form of radiation treatment using strongly interacting particles composed of quarks. The most common particles are protons, neutrons, and carbon ions. In 1904 William Bragg published curves demonstrating that the ionization density of alpha particles in air increases sharply near the end of range.[5] About 40 years later, in 1946, Dr. Robert R. Wilson described the fundamental physical feature depth-dose curve of heavy ions in compared to the X-rays (Figure 2) and proposed the idea that proton beam could be used for cancer treatment. [5] Protons were first used in therapy in the mid 1950's, followed by the first use of helium ions in 1957. In 1990 the first proton facilities have been established in clinical setting in Loma Linda University Center in California. [5]

In radiation treatment it is desirable to maximize the dose delivered in the tumour and, concurrently, to minimize the dose to the surrounding healthy tissue. During the conventional treatment with photons, most of the energy is transferred into tissues located at the surface and at shallow depths in the body, with an exponential decrease in dose with increasing depth (Figure 2), essentially with an unlimited range.[5] On the contrary, the physical properties of charged particles, as for instance protons, are finite beam range, near zero exit dose and sharp lateral penumbra. For 200 MeV protons (or 400 MeV carbon ions) the maximum penetration depth in the tissue is about 25 cm. [5]

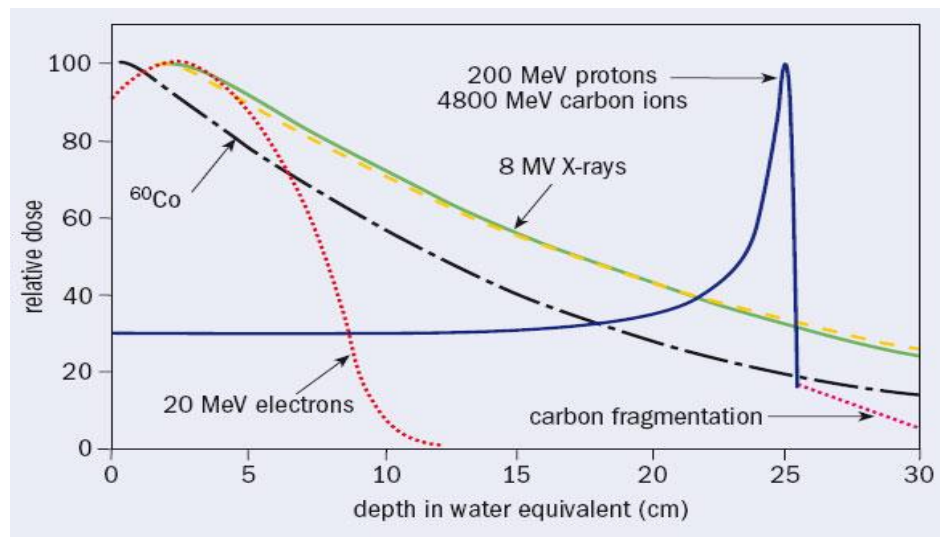


Figure 2: Comparison of the depth–dose relationships for heavy particles (carbon ions and protons) with electrons, X-Rays and gamma rays ^{60}Co . They have a significantly different depth dose curve which shows a narrow Bragg peak at the end for protons and carbon ions. [7]

The advantage of the Bragg peak is undisputed. Although the ion beam therapy solves many problems with the destruction of cancer cells, it is not a common procedure. The primary obstruction to a more widespread application is the high capital costs of proton therapy and the even higher cost of carbon-ion facilities. The whole system is significantly energetically expensive and the price of intervention derives from operating costs.

Since the year 1990 proton therapy for deep-seated tumors has become a common treatment. During the 20 years of development, there are above 5 types of proton therapy systems supplied by 6 companies controlling the world market. The attempts to reduce facility size and construction cost lead to the development of the new alternative. [6] There are several project based on the idea of treating cancer by laser driven ion beams. This type of treatment should bring cheaper and smaller constructions for future therapy centers. [6]

1.1. Biological Effectiveness

The number of ionized biomolecules per unit dose for protons, for heavier charged particles and for X-rays is similar, but the biological effects considerably differ. The quantity of cells surviving a particular dose of X-rays is larger than the quantity of cells surviving the same dose delivered by charged particles. RBE (relative biological effectiveness) is characterized by the ratio of the dose of 250 kVp X-rays or ^{60}Co gamma rays (well-known radiation standards) to the dose of tested radiation to produce the same effect. Effect may be represented by mutation, cell destruction, tissue damage, carcinogenesis or other effect on tissue and cells. [5]

Each value of particle energy has a slightly different effect on biological tissue. The energy transferred to the absorbing medium (tissue) per unit track length of the particle for monochromatic beams (characterized by the physical quantity linear energy transfer, LET), increases to a maximum as the particle's velocity slows near the end. Bragg peak is the term used for this narrow area where the LET reaches maximum values. [5]

2. Physical Principles

2.1. Lorentz Force

The trajectory of charged particle can be influenced by combination of electric and magnetic fields through the Lorentz force

$$\mathbf{F}_L = \mathbf{F}_e + \mathbf{F}_m = q\mathbf{E} + q(\mathbf{v} \times \mathbf{B}), \quad (1)$$

where q is an electric charge with instantaneous velocity, \mathbf{B} is magnetic field, \mathbf{E} is external electrical field and \mathbf{v} is velocity of charged particle. [8]

The path of charged particles can be predicted based of the knowledge about the location and amplitudes of electric and magnetic fields. The force is always perpendicular to the velocity \mathbf{v} and the magnetic field \mathbf{B} . If the particle is stationary, then the magnetic field is zero.

For relativistic particles whose velocity $\mathbf{v} \approx c$ the Lorentz force from magnetic field $\mathbf{B} = 1 \text{ T}$ is the same as from an electrical field $\mathbf{E} = 300 \text{ MV/m}$. As a practical result, it is preferable to use magnetic fields to deflect or focus relativistic charged particles. [8]

The Lorentz force provides the centripetal acceleration, which is necessary for particle to move in circle perpendicular to the magnetic field direction Figure 3.

$$\mathbf{F}_L = \frac{mv^2}{r} \quad (2)$$

Where m is a mass, v is the velocity of the mass, r is radius of curvature. [9]

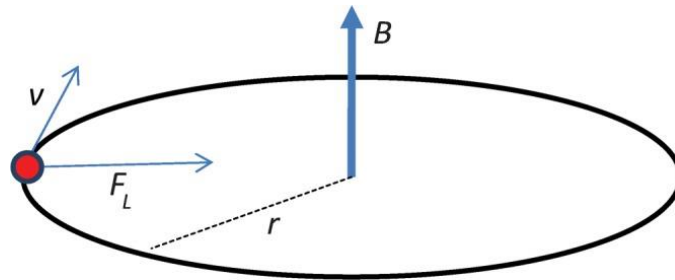


Figure 3: Deflection of the particle for $\mathbf{v} \perp \mathbf{B}$ [9]

2.2. Kinetic Energy

The value of kinetic energy depends on the velocity \mathbf{v} and the particle mass m . According to Newtonian classical mechanics the kinetic energy is defined as:

$$KE = \frac{1}{2}m\mathbf{v}^2. \quad (3)$$

The unit for energy is $\text{kg} \cdot \text{m}^2 \cdot \text{s}^{-2}$ or Joule. This physical relationship is, however valid only for small velocity $\mathbf{v} \ll \mathbf{c}$. In relativistic case we have to work with Einstein's formula, where the rest energy is defined as:

$$E_0 = m\mathbf{c}^2. \quad (4)$$

Total energy E is defined as:

$$E = \gamma m\mathbf{c}^2, \quad (5)$$

where m is the mass of the particles in rest (rest mass), \mathbf{c} is a speed of light. The apparent mass of a particle changes with a γ (Lorentz factor). The Lorentz factor γ is:

$$\gamma = \frac{1}{\sqrt{1 - \frac{\mathbf{v}^2}{\mathbf{c}^2}}} = \frac{1}{\sqrt{1 - \beta^2}} = \frac{dt}{d\tau}, \quad (6)$$

where \mathbf{v} is the relative velocity of the particle in the reference frame, \mathbf{c} is the speed of light in vacuum, β is the ratio of \mathbf{v} and \mathbf{c} , t is coordinate time and τ is proper time for an observer. Proper time τ of an observer is the time shown on the observer's own clock. For understanding the derivation of the relationship for Lorentz factor, it is necessary to study time dilation. [10]

To obtain the formula for relativistic kinetic energy, we start from the rest energy (eg. 4), and then we get the equation for relativistic kinetic energy KE_{rel} as the difference from the total energy (eq. 5). [11]

$$KE_{rel} = E - E_0 = \gamma m\mathbf{c}^2 - m\mathbf{c}^2 = (\gamma - 1)m\mathbf{c}^2 \quad (7)$$

To show that the classical expression for kinetic energy is obtained at low velocities of mass, the first order binomial expansion for γ at low velocities gives:

$$\gamma = 1 + \frac{1}{2} \frac{v^2}{c^2} \quad (8)$$

Introduced into the formula for relativistic kinematic energy gives

$$KE_{rel} = \left[\frac{1}{2} \frac{v^2}{c^2} \right] mc^2 = \frac{1}{2} mv^2 = KE_{class} . \quad (9)$$

If the velocity v is much smaller than speed of light c , the relativistic kinetic energy has the same progress as the classic kinetic energy (the Lorentz Factor is near to 1). This is apparent from Figure 4. The speed of the light is the ultimate speed limit for every particle with a non-zero rest mass. The velocity of the particle can only approach the speed of the light, but not reach it. [11]

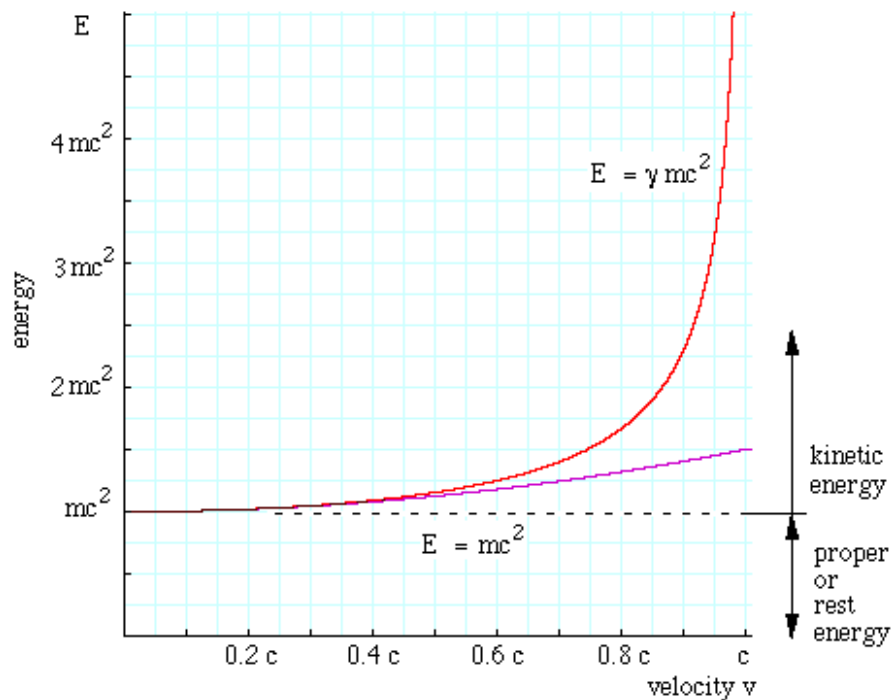


Figure 4: The purple line shows the classical kinetic energy and the red line the relativistic kinetic energy. [12]

2.3. Conventional acceleration

The first accelerators used high voltage produced by a Van de Graaf generator, which uses a moving belt to accumulate very high amounts of electrical potential on a hollow metal globe on the top of the stand, which are able to produce over 5MV. [13]

Particles inside modern accelerators are able to reach almost the speed of light $c = 299,792.458$ km/s. According to Einstein's theory, this speed cannot be exceeded by any particle. The difference, between less and more powerful accelerator, is in the maximum kinetic energy of the charged particle that can be reached. [13]

The energy is a measure of the accelerator's power; the unit is electron volt (eV). Electron volt is a unit of energy equal to approximately $1.602 \cdot 10^{-19}$ Joule. According to the definition one eV corresponds to the amount of energy gained by the charge of electron moved across an electric potential difference one volt. 1 GeV is almost the energy equivalent to the rest mass of proton, considering the relation $E = mc^2$. The Large Hadron Collider, currently the largest particle accelerator, which is located in CERN, is able to accelerate protons up to the kinetic energy of 7 TeV ($7 \cdot 10^{12}$ eV). If we convert this number into joules, we obtain $7 \cdot 10^{12} \cdot 1.602 \cdot 10^{-19} = 11.2 \cdot 10^{-7}$ J per particle. [14]

2.3.1. Cyclotron

The first cyclotron was constructed in 1930 by E. Lawrence, who laid the foundation for modern particle acceleration. A cyclotron consists in a strong circular electromagnet with a constant magnetic field, a voltage source of high frequency, and a pair of large electrodes with a D shape (known as dees). In the gap between both dees there is a uniform electric field. Charged particles are introduced near to the centre of the cyclotron. [9]

If charged particles with a non-zero velocity are inside a static magnetic field (inside dee), the Lorentz force bends the particles path in a circle. The magnetic field is perpendicular to the direction of their motion. The particle is influenced only by a magnetic field, because it is shielded from the electric field inside the dee, which acts as a Faraday cage. [9]

The particles are accelerated only in the gap between dees, because there is a potential difference. During the time that particle is inside, the polarity is inverted, so that the vector of electric field in the gap has the same orientation with respect to the velocity vector of the particle. Each time the particle crosses the gap, it gains a small increment in kinetic energy and moves outwards to an orbit with a large radius. The sequential succession of gap crossings causes the particle to move in spiral, until it is extracted and transported through the beamline. Switching of the polarity of the dees is facilitated by an alternating current source with a frequency in the megahertz range (usually referred to as radiofrequency, RF). The scheme of a cyclotron is shown in Figure 5. [9]

As the velocity of the particle approaches the speed of light, it is necessary to work with an effect of relativity. A proton accelerated to 250 MeV, will move with 60% of speed of light. [9]

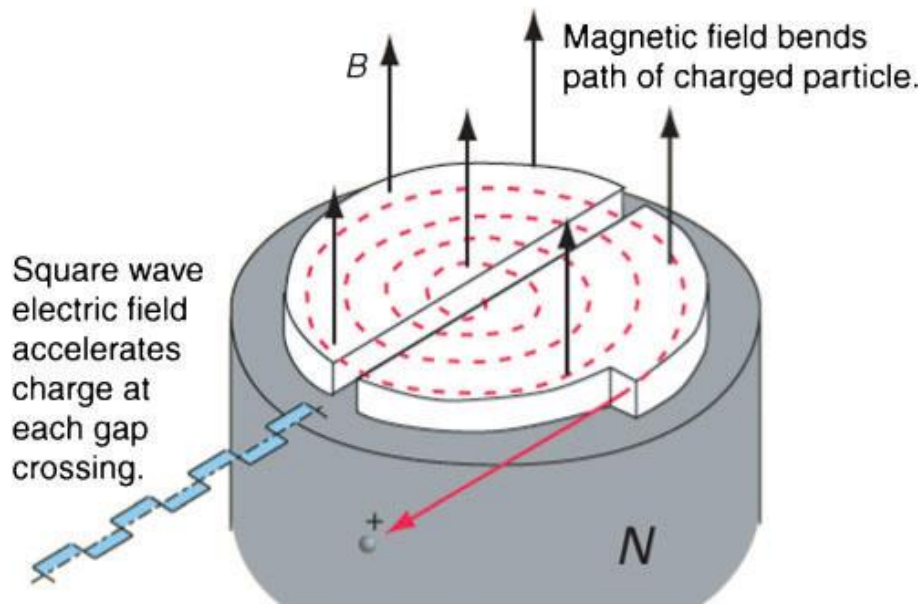


Figure 5: Scheme of cyclotron [9]

2.3.2. Linear Particle Accelerator

A linear particle accelerator (known as *linac*) increases the kinetic energy using a straight evacuated chamber by an electric field oscillating with a constant radio frequency (RF). The charged particles are exposed to longitudinal electrical field and they are accelerated by the electrostatic field in the gap between the electrodes. Although modern linacs use continuous RF vacuum cavities, the principle of acceleration is more easily understood with linacs of older design, where cylindrical electrodes called drift tubes are used in their construction. They are aligned coaxially with the vacuum chamber.

The tube in front of the particles has opposite charge with respect to the particles (e.g. electrons need positive potential), therefore the particles are attracted. Once the particles are inside the tube, the polarity is reversed. The particles inside the tube are shielded from electric field (Faraday cage). The continually reversed polarity ensures that the charged particle is continually attracted to the opposite charged electrode. If the polarity of the electrode did not change, the particles would decelerate and loose their kinetic energy. As the particle energy and velocity increase, a longer drift tube is necessary as we can see in Figure 6. [15] Since the number of cavities in the linac is not limited, with a sufficiently long linac, charged particles can be accelerated to significantly larger energies than is their rest mass.

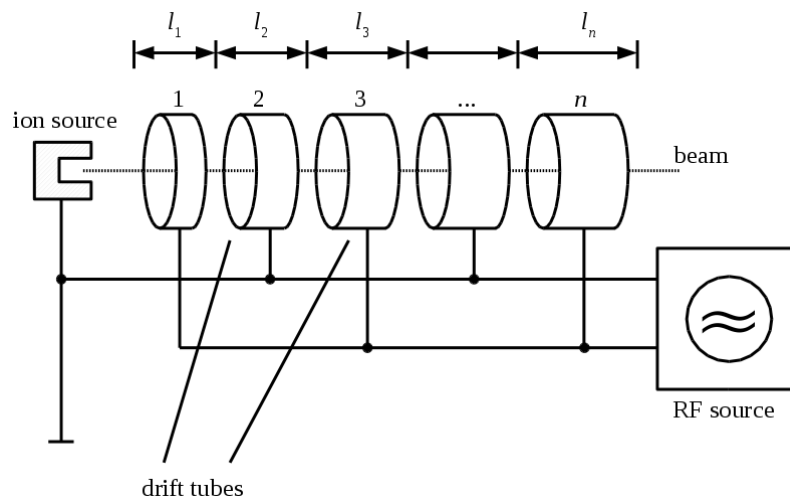


Figure 6: Scheme of linear accelerator [16]

3. Laser-driven Proton Acceleration

As mentioned before, the protons need a large cyclotron or synchrotron to be accelerated. However, the high investment and maintenance cost of the proton therapy infrastructure is limiting its widespread use.

The emerging option of laser acceleration may solve these problems. The main advantages of the novel proton accelerators is that the system for acceleration is envisaged as very compact and the investment costs can thus be substantially lower compared to a conventional proton facility.

Over the last decades several acceleration regimes have been studied, such as Target Normal Sheath Acceleration (TNSA), Coulomb Explosion, Radiation Pressure Acceleration (RPA), Magnetic Vortex Acceleration and Shock Wave Acceleration.[17] A proton beam with energy around several tens of MeV can be produced from interaction of ultra-intense (more than 10^{18} W/cm²) short pulse (between 30 fs – 10 ps) laser with thin solid foils. [17]

Contrary to the conventional accelerators the laser produced proton beam is characterized by a large divergence ($\pm 25^\circ$) and a huge energy spread (100%), its only positive feature being its small transverse emittance (usually the beam spot is less than 1 mm).

For this reason it is necessary to construct an energy selector system (ESS) that will be able to choose the energy needed for the particular irradiation case. The main goal of the transport system is to collect most of the beam to maximize the transmission efficiency and to optimize the energy selection. [18]

3.1. Chirped Pulse Amplification (CPA)

In order to accelerate protons to very high kinetic energies using laser pulses, these pulses must be both very short and contain sufficient amount of energy. A laser is a device that emits light through a process of optical amplification based on the stimulated emission of electromagnetic radiation. In a high-power pulsed laser system a short pulse of small energy is amplified several times in a separate dedicated amplification medium. However, during the amplification process for ultrashort optical pulses, the optical peak intensities can become very high. This could lead to detrimental nonlinear pulse distortion or even destruction of the gain medium. [19]

Chirped Pulse Amplification (CPA) is a technique that permits the amplification of ultrashort laser pulses to high energy levels without damage to the amplifier medium. CPA is based on the extension/stretching of a chirped laser pulse (the term *chirped* comes from radar terminology and denotes a pulse consisting of band of different frequencies/wavelengths) on a pair of optical gratings before it enters the amplifier and its subsequent compression on a different pair of gratings after the amplification is complete. [19]

The CPA method allows the construction of a compact high-power laser with peak power of several terawatts or higher. Modern CPA lasers are usually based on Ti-Sapphire or Nd-Glass crystals and consist of the following main parts: femtosecond oscillator, stretcher, amplifier, compressor and focusing system. The schematic picture of CPA technique is depicted in Figure 7. [19]

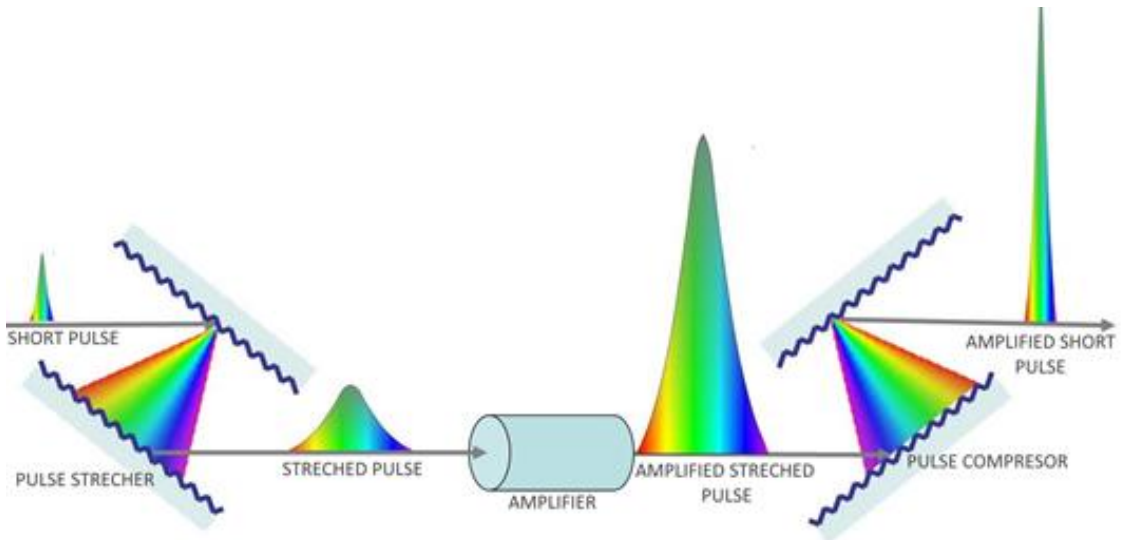


Figure 7: Principal components of CPA laser system (edited from [20]).

3.2. TARANIS Laser System

The ESS prototype was tested at the laser system TARANIS (Terawatt Apparatus for Relativistic and Nonlinear Interdisciplinary Science) in Belfast, where the images of photoluminescence plates for experimental data were taken. The multi terawatt TARANIS system operated with a CPA mode, as was described in the previous chapter 3.1. [21]

The laser TARANIS is a hybrid Ti:Sapphire-Nd:glass system, which can simultaneously deliver two beams of photons with a fundamental wavelength of 1053 nm and a repetition rate of 1 shot every 10 min. The duration of the laser pulses can be specified in the range from 700fs to 1ns. The intensities at the target can reach 10^{19} W/cm². [21]

The laser system has two target areas, each of which can be illuminated with a combination of the two different combinations of laser pulses. The first target area is usually mainly used for investigation of X-ray lasers. The second target area can be used for experiments on laser-driven particle acceleration, X-ray sources, and other applications. The experimental setup for laser-driven acceleration was adjusted so that the beam focused on a thin aluminium foil of a thickness from 0.7 to 100 μ m. Energy delivered on the target was ~ 7 J and the pulse was ~ 560 fs in duration. The focal spot diameter measured in the low power was about 10 μ m and the laser intensity on the target was on the order of 10^{19} W/cm². [21]

3.3. TNSA Regime

The most commonly used regime that is used for laser-driven acceleration is known as Target Normal Sheath Acceleration (TNSA). The TNSA principle is based on high intensity laser – matter and plasma interactions with thin solid foils. Plasma is defined as a highly ionized gas containing an approximately equal number of positive ions and electrons with total zero charge.

A basic principle of TNSA is depicted in Figure 8. At the beginning of TNSA, a high intensity laser pulse hits a thin metal foil. At the front side of the target hot plasma is created; in the plasma, electrons are accelerated. Electrons passing through the thin foil are gathered and trapped at the back of the target, where the Coulomb force counteracts the charge separation. This electrostatic field accelerates protons as they are attracted by electrons.

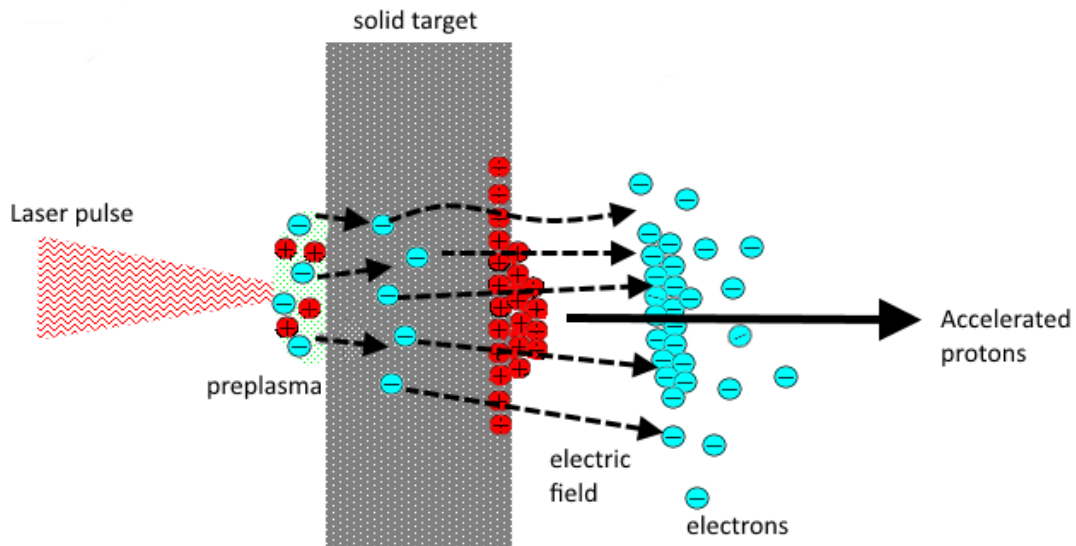


Figure 8: Principle of TNSA regime

A thin foil target is used, with a thickness of about 10 microns, to reduce the transverse spreading of the hot electrons inside the target. The maximum expected kinetic energy of proton beams accelerated by TNSA regime is about 60 MeV. The required laser

intensities on the target for such proton energies are about 10^{21} and 10^{22} W/cm². The next generation laser facilities (e.g. ELI) are designed to deliver such intensities and help to further develop in the different acceleration mechanism investigation. [22]

Proton beams accelerated by TNSA have a broad energy distribution, which can be explained by three ways. The first possible option is that the accelerating field is inhomogeneous in transversal direction, which means that the proton located in the middle of the field are accelerated more, whilst protons outside of the centre are accelerated to lower energies (Figure 9). Secondly, the broad distribution can be caused by screening effects. Protons deeper in the layer are shielded by electric field by particles with higher speed. The last possibility is that the TNSA field may need some time to reach the maximum field strength. [22]

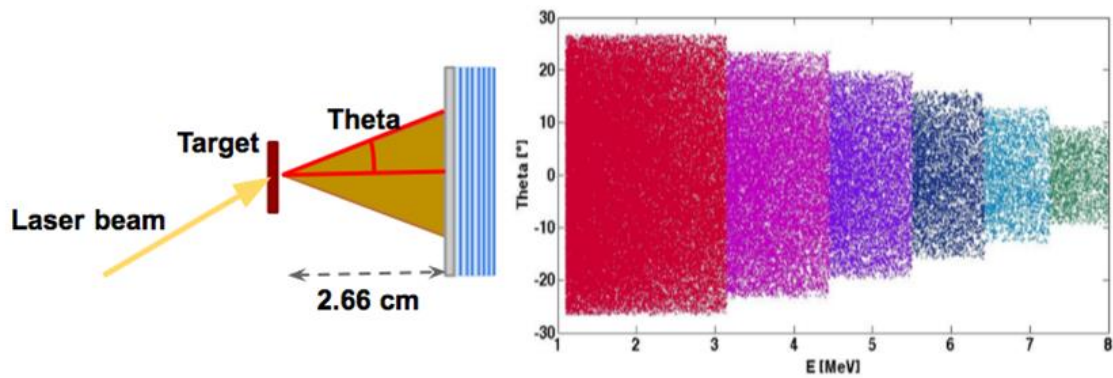


Figure 9: Angular distribution. (The picture was taken with permission from presentation ‘Transport beamline solutions for laser – accelerated proton beams’ by A. Tramontana).

Because of the broad distribution, the application for the medical field is still problematic. It is necessary to select the proton energy that can be used for radiation treatment at a desired depth. The selection of the required proton energy can be performed by means of a device, which is able to separate the particle trajectories according to their energies and select a desired value energy penetration depth. However, it is important to admit that there are other issues, which need to be solved with laser-based proton acceleration, like the extension of the maximum energy cut-off of the particles and the stability and the reproducibility of the proton beam parameters. To achieve some of these goals, it will be necessary to increase the laser pulses intensity on target. [23]

3.4. The Energy Selector System

TNSA regime produces polychromatic highly divergent proton beams. Medical applications, however, need a controlled and monochromatic beam in order to precisely determine the dose released. For this reason, a first prototype of an energy selector system (ESS) for laser driven proton beams has been designed and calibrated at the Laboratori Nazionali del Sud (LNS) in Catania. The ESS is able to select the required proton's energy.

The ESS is one of the most important components of the beam transport line. It is a very compact system that may allow reducing the massive transporting system typically used in conventional proton therapy. [17]

The ESS consists of four dipole magnets with alternating polarity that provide the spatial separation of the charged particles with different energies. The second and third magnetic fields are parallel with each other and the first and fourth magnetic fields are oriented in the opposite direction with respect to the second and the third one. The laser-accelerated proton beam enters the first magnetic dipole and in the first two dipoles is horizontally spectrally dispersed. A moveable slit is used to let particles of a narrow energy range enter the deflecting sector while the others are stopped. The protons passing through the collimator's slit are refocused by opposite gradient of the third and fourth dipoles. With varying position of two central dipoles and the slit it is possible to select the desired energy spectrum. [17]

Schematic drawing of the ESS is shown in Figure 10 and a 3D model of the ESS is presented in Figure 11. The four dipoles are situated on a platform about 65 cm long and 20 cm wide. Each neodymium (NdFeB) magnet has size of 88 mm (L) x 142 mm (W) and produces magnetic field of about 0.85 T. The gaps between the 1st and the 2nd dipole and between 3rd and the 4th dipole are both 85 mm wide. The distance between 2nd and 3rd dipole is 10 mm. Two collimators (see in Figure 11) are designed to control the spatial profile of the proton beam. In Figure 12, the approximate trajectories of protons with different energies inside the ESS are shown. Particles with lower energies are deflected further away from the incoming axis and particles with higher energies are closer.[17]

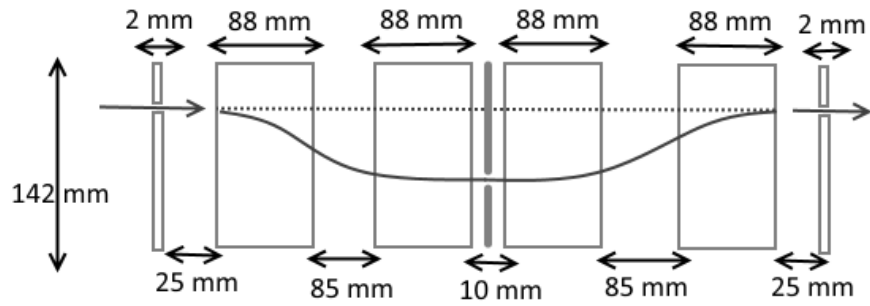


Figure 10: Schematic drawing of prototype energy selector system constructed in Catania and tested in TARANIS with dimensions.

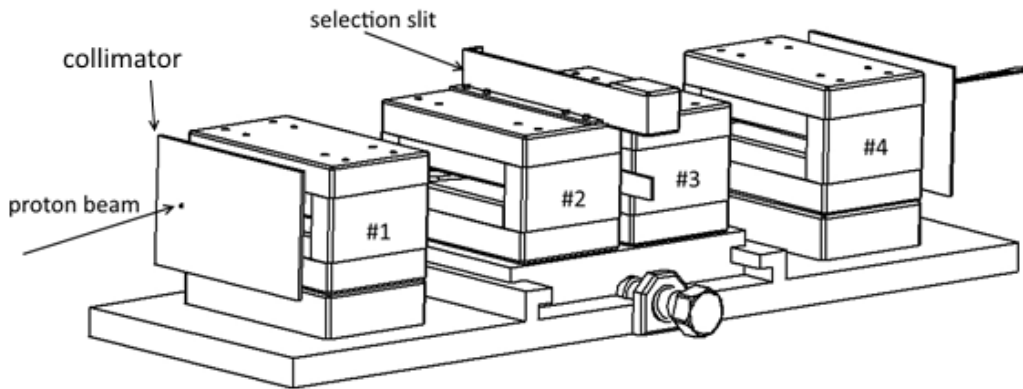


Figure 11: 3D model of energy selector system made in program SolidWorks

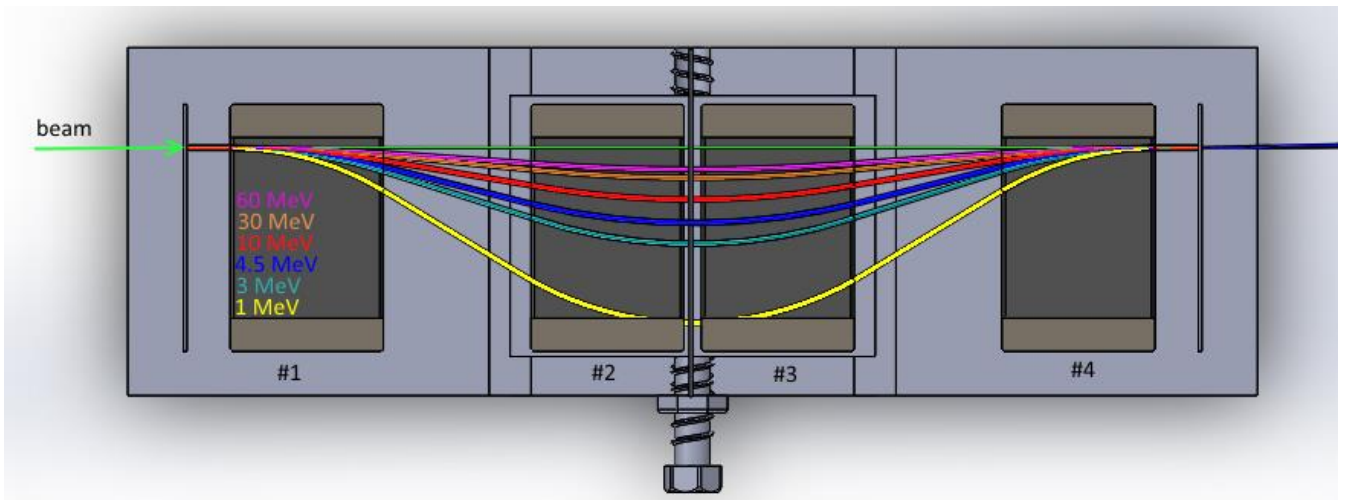


Figure 12: 3D model of energy selector system from top view of the particle trajectories at different energies.

4. Experimental Data

4.1. Imaging Plate

There are many types of detectors, which are used to record high energy protons produced in laser matter interactions (e.g. solid state nuclear track detectors such as CR39, scintillators crystals, Cherenkov detectors, microchannel plates, Faraday cups or imaging plates). In our experimental setup imaging plates (IPs) were used – these are phosphor films very sensitive to ionizing particles. [24]

The IPs can provide information about the spatial profile of the proton beams. Particles, which are produced at ultrahigh intensity laser facilities with laser-target interaction, require a diagnostic system capable of measuring proton pulses of very high particle flux and very short duration. The imaging plates were chosen for their exquisite sensitivity to low-energy protons and their insensitivity to magnetic field. [24]

Imaging plates are made of 3 or 4 layers: a protective layer, a phosphor layer, a support layer, and a magnetic layer, which is optional. The exposure of IP is similar to a photographic film. The IP is scanned with a red light laser beam and after the exposure it could be erased with white light and used again. Because the intensity of the laser-stimulated photoemission decreases with post-irradiation time, it is necessary to scan the IP at the same time after the proton exposure. [25]

4.2. Geometry of Beam Trajectory in ESS

As mentioned in chapter 3.4, the prototype of the energy selector system is composed of four permanent dipoles with alternating polarity. The spatial profile of the magnetic field along the beam axis was measured by using a Hall probe to verify the spatial uniformity of the magnetic field. The magnetic field on the bending plane of each dipole was measured with mean value of about 0.85 T, although small deviations are present, as can be seen in Figure 13. The position of the incoming beam is 10 mm from the left edge of the left aluminium pinhole screen placed 25 mm upstream from the ESS.

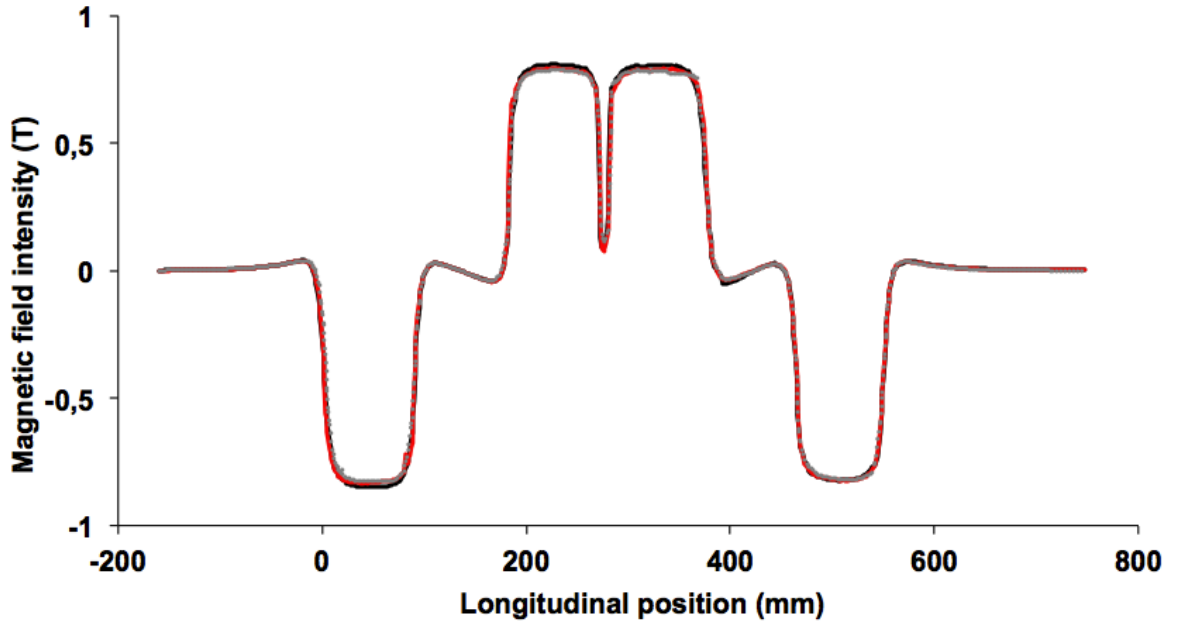


Figure 13: Magnetic field profiles measured along the radial plane [17]

Assuming that the dipoles are identical rectangular magnets and that the axis of the incoming beam is parallel to the axes of the dipoles, we can geometrically express the proton path inside the ESS (see in Figure 14). The length of the magnetic dipole l_{eff} can be related to the bending radius r and the bending angle α using a simple trigonometrical relation as:

$$l_{eff} = r \cdot \sin \alpha \quad (10)$$

The length of proton trajectory inside the magnetic dipole l_{arc} can be calculated as the length of circular arc:

$$l_{arc} = r \cdot \alpha \quad (11)$$

$$l_{arc} = l_{eff} \cdot \frac{\alpha}{\sin \alpha} \quad (12)$$

The transverse displacement of the proton's path inside the dipole x_{arc} is given by the equation:

$$x_{arc} = r - r \cdot \cos \alpha = r \cdot (1 - \cos \alpha) \quad (13)$$

$$x_{arc} = \frac{l_{eff}}{\sin \alpha} \cdot (1 - \cos \alpha) = l_{eff} \cdot \frac{1 - \cos \alpha}{\sin \alpha} \quad (14)$$

The deflection x_d of the proton beam in the horizontal direction within the gap of the width d between the dipoles is:

$$x_d = d \cdot \tan \alpha \quad (15)$$

The position of the selection slit Δx can be obtained as sum of the deflection of the proton beam inside the first two dipoles (that are identical) and in the gap between the dipoles.[26]

$$\Delta x = 2 \cdot x_{arc} + x_d \quad (16)$$

$$\Delta x = 2 \cdot l_{eff} \cdot \frac{1 - \cos \alpha}{\sin \alpha} + d \cdot \tan \alpha \quad (17)$$

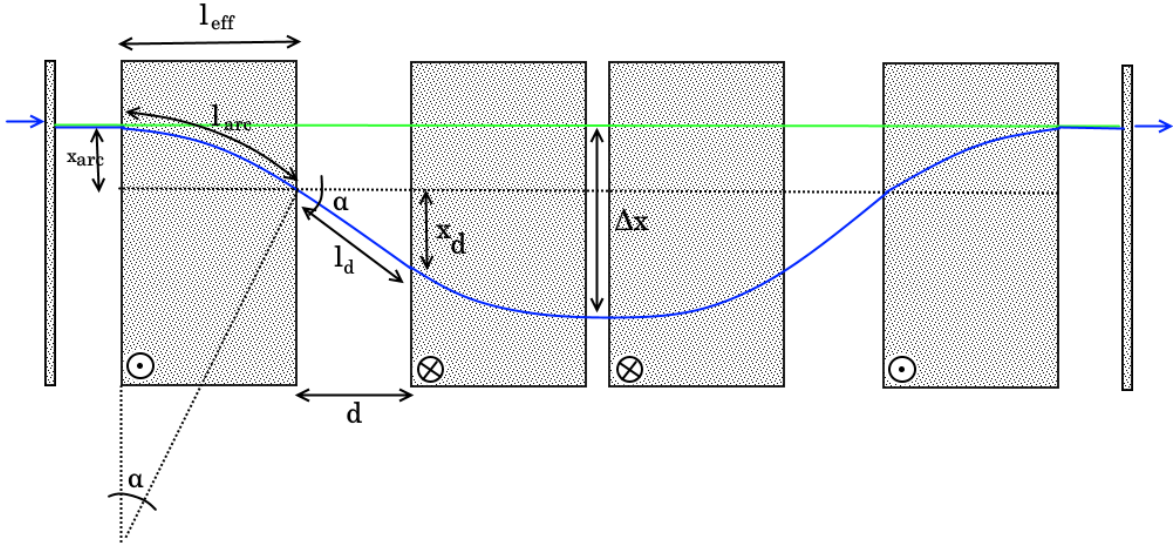


Figure 14: Schematic diagram of the proton beam trajectory inside energy selector system. (r - bending radius, α - bending angle, x_{arc} - transverse displacement, l_{arc} - length of the trajectory, l_{eff} - effective magnetic field length, d is a measure of gap between the first and the second dipole, l_d is length of the proton beam's path outside the dipole and x_d is deflection of the proton beam in horizontal direction outside the dipole).

4.3. Position of Selection Slit

The dispersion of different proton energies achieved while passing through the ESS was described in the previous chapter. To select the desired proton energy we need to calculate its horizontal position between the second and the third dipole relative to the incoming position. Then we proceed with placing a slit into the acquired position to perform the actual selection.

The total relativistic energy is the sum of kinetic energy and rest energy according to equation 7 for chapter 2.2.

$$E = KE_{rel} + E_0 \quad (18)$$

As an example, since the mass of a proton is $m_p = 938 \text{ MeV}/c^2 = 1.673 \cdot 10^{-27} \text{ kg}$ a proton with kinetic energy 4.5 MeV has a total energy $E = 938 + 4.5 = 942.5 \text{ MeV}$. The Lorentz factor is $\gamma = \frac{E}{mc^2} = \frac{942.5}{938}$ and the velocity is $\beta = \frac{v}{c} = \sqrt{1 - \gamma^{-2}} \approx 0.0976$.

Relationships (1) and (2) for Lorentz force from chapter 2.1 can be combined to get the equation for the bending radius r :

$$r = \frac{v \cdot m}{B \cdot q} = \frac{\beta \cdot c \cdot m}{B \cdot q} \quad (19)$$

Substituting for magnetic intensity $B=0.85$ T, elementary electric charge $q = 1.602 \cdot 10^{-19}$ C and proton mass m_p in kg, the resulting bending radius is 360 mm. Dimensions of ESS are shown above in chapter 3.4 in Figure 10, $d = 85$ mm and $l_{eff} = 88$ mm. From equation (10) the bending angle α can be calculated to be:

$$\alpha = \arcsin\left(\frac{l_{eff}}{r}\right) = \arcsin\left(\frac{88}{360}\right) = 14.15^\circ \quad (20)$$

According to equation 17, the required position of the slit for selection of protons with kinetic energy of 4.5 MeV can be obtained as $\Delta x = 43$ mm. By plotting the dependence of the slit position on the required proton energy a calibration curve of the ESS was determined (see in Figure 15).

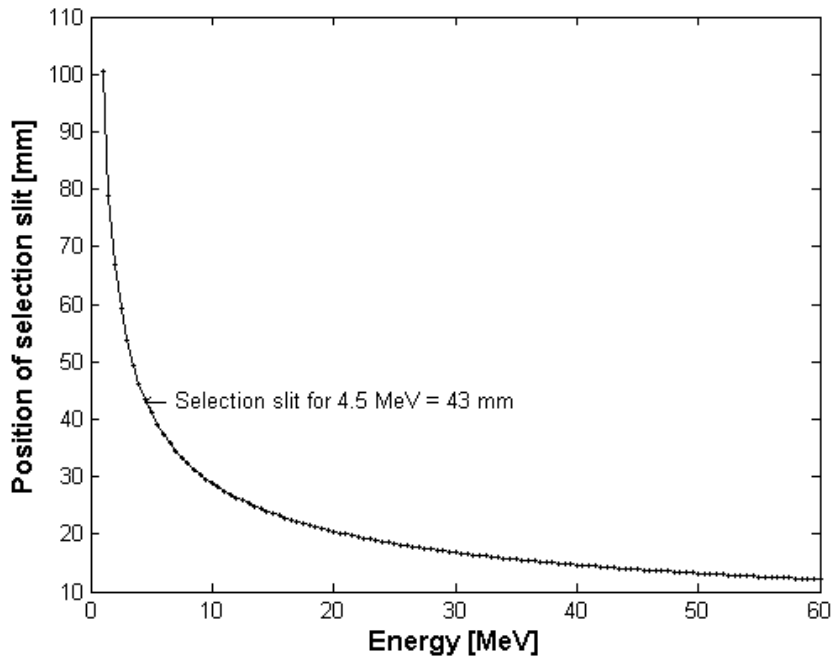


Figure 15: The position of selection slit according to required energy of protons

4.4. Output Beam Angle

Imaging plates were used as detectors placed either 30.9 or 41.9 cm behind the last collimator. Their position is shown in Figure 16. Imaging data from the energy selector system were collected during experimental test performed at the TARANIS facility. The following work with experimental data was performed using the Image J software in order to process the images and determine the output angle of ESS.

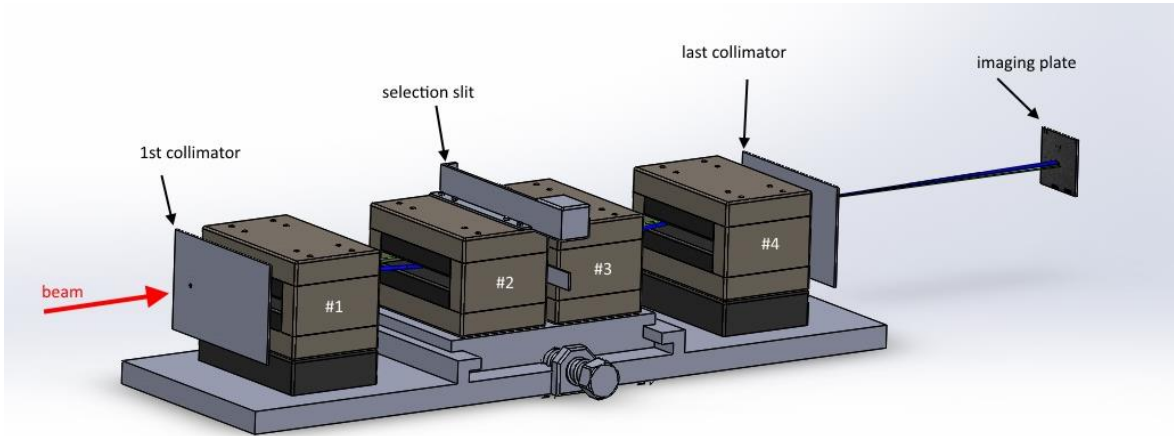


Figure 16: 3D model of experimental ESS with IP detector

4.4.1. First Shot

The first shot was made for selection slit placed in position to select protons of the energy of 4.5 MeV. The size of the slit was 3 mm width and 6 mm height. An image plate was placed at 30.9 cm from the final collimator. As is indicated in Figure 17, green light laser was used to mark the original primary axis of the proton beam on the luminescence plate (Figure 18) to allow measurements of the relative deviation of the proton beam from the primary path.

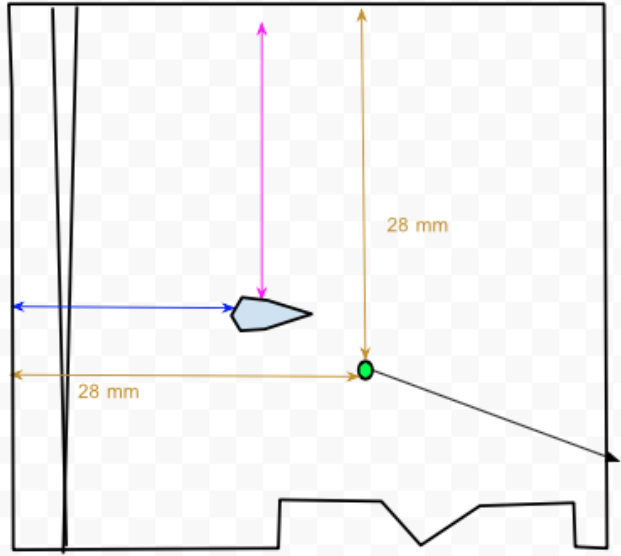


Figure 17: A scheme of location of green point laser on a luminescence plate.

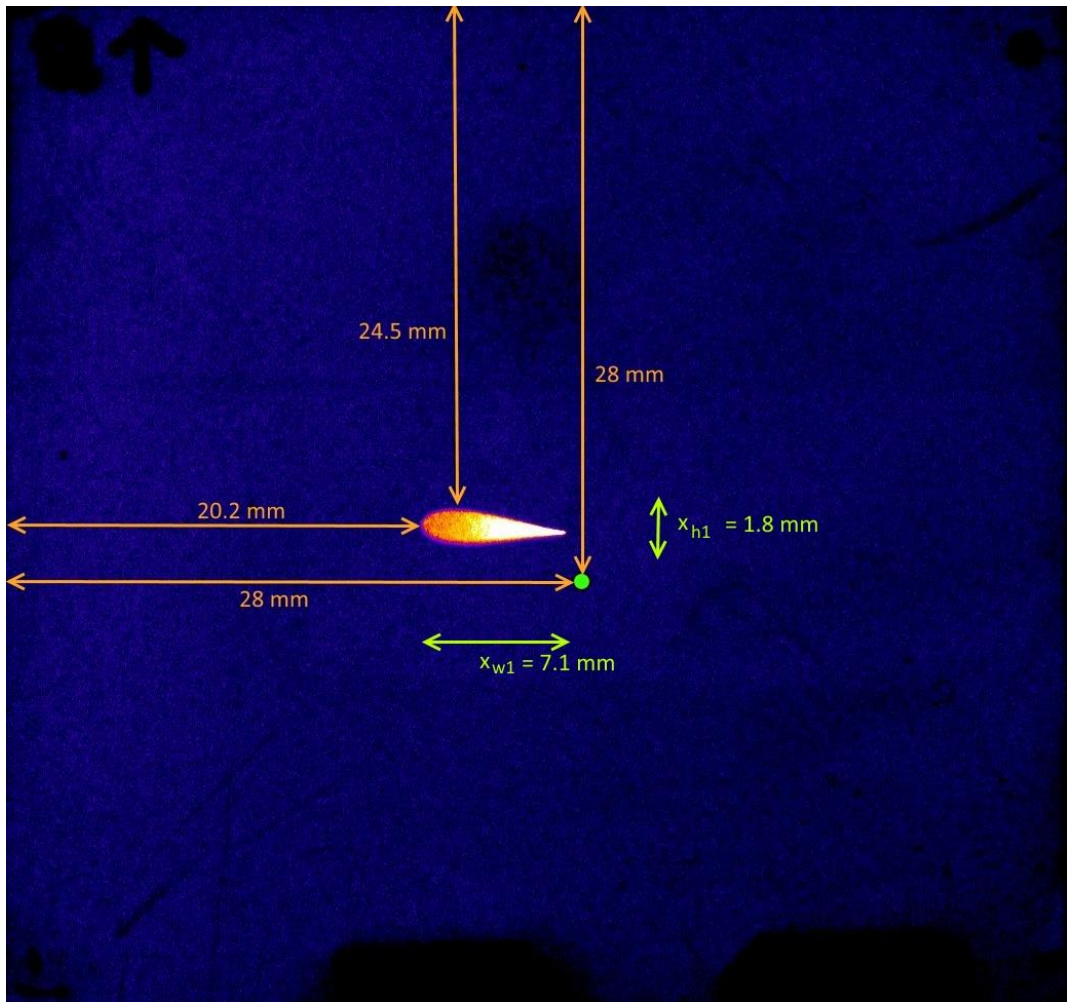


Figure 18: A picture of the luminescence plate with marked dimensions of the first shot.

4.4.1.1. Vertical direction

Using trigonometric functions, the output angle and the divergence of the beam in vertical directions was calculated. Figure 18 shows the measured distances and Figure 19 provides a schematic picture of the beam spot location.

$$x_{ver1} = 28 \text{ mm} - 24.5 \text{ mm} = 3.5 \text{ mm}$$

The output angle in vertical direction can be obtained from the tangent identity (tangent equals opposite over adjacent). The opposite is equal to the value x_{ver1} and the adjacent is equal to a distance between the imaging plate and the final collimator, which is $l_{IP1} = 30.9$ cm. Substituting the correct values we obtain the value of the angle θ_1 , which corresponds to a deflection angle in the vertical direction.

$$\tan \theta_1 = \frac{x_{ver1}}{309} = \frac{3.5}{309}$$

$$\theta_1 = 0.65 = 0^\circ 39'$$

In the next step, we can calculate the divergence δ_1 in vertical direction from the measured proton beam height $x_{h1} = 1.8$ mm. In the following example we used the law of sines.

$$\frac{x_{h1}}{\sin \delta_1} = \frac{\sqrt{(x_{ver1} - x_{h1})^2 + l_{IP1}^2}}{\sin(90^\circ - \theta_1)}$$

$$\frac{1.8}{\sin \delta_1} = \frac{\sqrt{(3.6 - 1.8)^2 + 309^2}}{\sin(90^\circ - 0.65^\circ)}$$

$$\delta_1 = 0.34^\circ = 0^\circ 20'$$

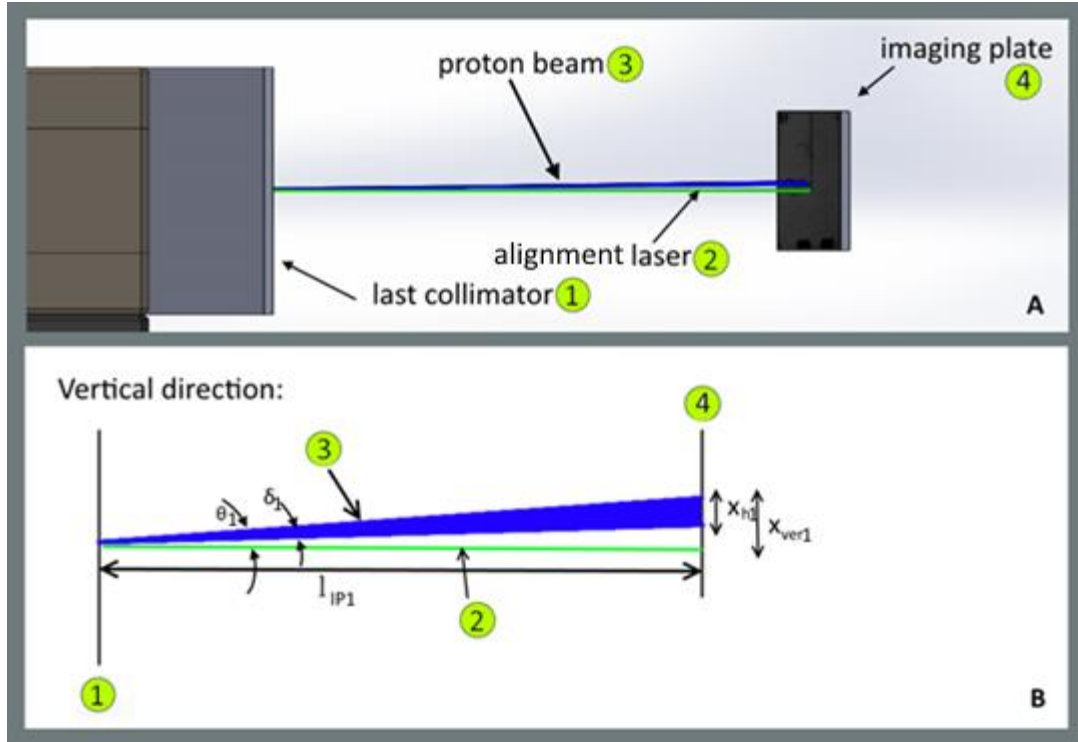


Figure 19: A) Side view of the ESS output with visualised data from Imaging plate for detector, shot #1, B) The scheme of the vertical deflection of the proton beam from the path of the alignment laser (1 - final collimator, 2 - alignment laser, 3- proton beam, 4 - imaging plate, l_{IP1} – distance from the last collimator to the imaging plate, x_{h1} – height of the proton beam, x_{ver1} – vertical displacement of the proton beam, θ_1 – angle between the alignment laser and the proton beam, δ_1 – divergence of the proton beam)

4.4.1.2. Horizontal direction

As in the previous case for the vertical direction, we were able to calculate the output angle and the divergence in the horizontal directions. In Figure 18, the measured distances are shown, while Figure 20 shows the schematic of the beam spot location.

$$x_{hor1} = 28 \text{ mm} - 20.2 \text{ mm} = 7.8 \text{ mm}$$

The output angle in horizontal direction can get from the tangent identity. Opposite is equal to the value x_{hor1} and adjacent is equal to a distance between the imaging plate and the final collimator, which is $l_{IP1} = 30.9 \text{ cm}$. Substituting in the correct units we obtained the angle φ_1 , which is a deflection in the horizontal direction.

$$\tan \varphi_1 = \frac{x_{hor1}}{309} = \frac{7.8}{309}$$

$$\varphi_1 = 1.45 = 1^\circ 26'$$

Next, we are able from the measured proton beam width $x_{w1} = 7.1$ mm to obtain the divergence ψ_1 in horizontal direction.

$$\frac{x_{w1}}{\sin \psi_1} = \frac{\sqrt{(x_{hor1} - x_{w1})^2 + l_{IP1}^2}}{\sin(90^\circ - \varphi_1)}$$

$$\frac{7.1}{\sin \psi_1} = \frac{\sqrt{(7.8 - 7.1)^2 + 309^2}}{\sin(90^\circ - 1.45^\circ)}$$

$$\psi_1 = 1.32^\circ = 1^\circ 19'$$

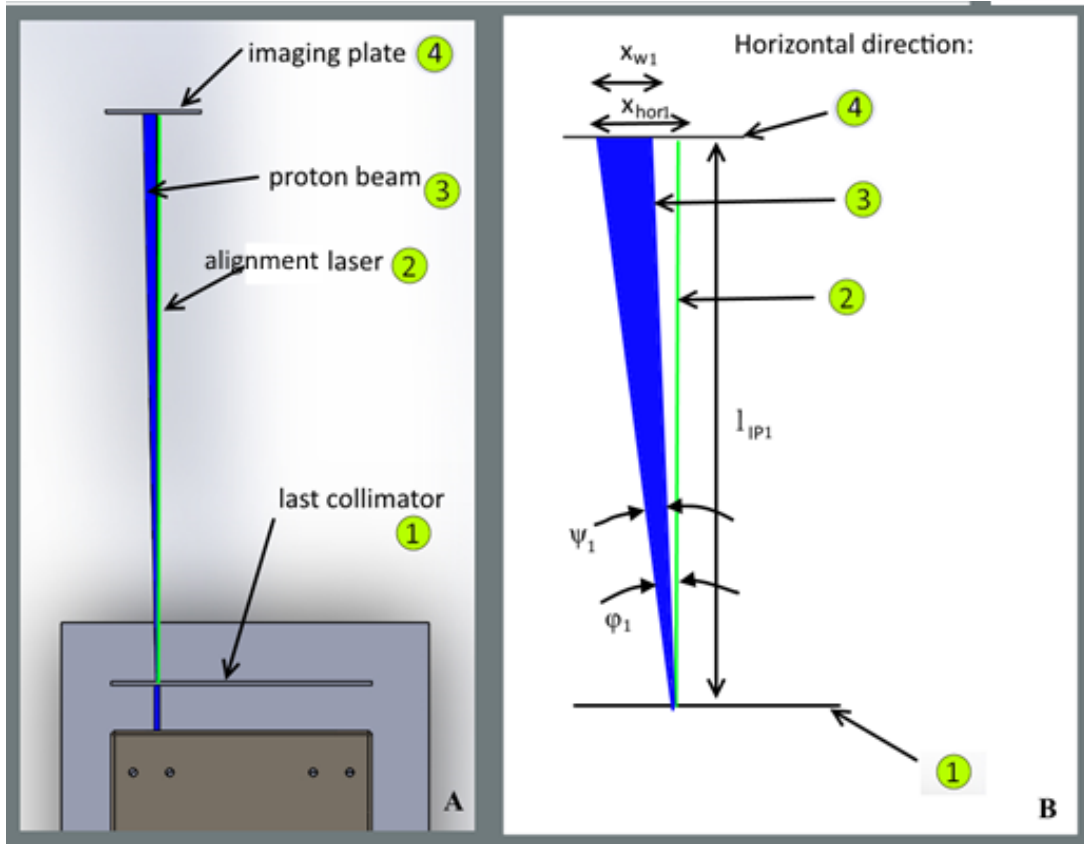


Figure 20: A) Top view of the ESS output with visualised data from Imaging plate for detector, shot #1, B) The scheme of the horizontal deflection of the proton beam from the alignment laser. (1- final collimator, 2- alignment laser, 3- proton beam, 4- imaging plate, l_{IP1} – distance from last collimator to imaging plate, x_{w1} – width of the proton beam, x_{hor1} – horizontal displacement of proton beam, φ_1 – angle between proton beam and alignment laser, ψ_1 – divergence of proton beam)

4.4.2. Second Shot

The same procedure was applied for the second shot, which was made for selection slit placed in position to select energy 4.5 MeV, the size of slit was 3 mm width and 6 mm height. An image plate was placed at 30.9 cm + 11 cm from the final collimator. As is indicated in Figure 21, a green light laser was used to mark the original primary axis of the proton beam on the luminescence plate (Figure 22) to allow measurements of the relative deviation of the proton beam from the primary direction.

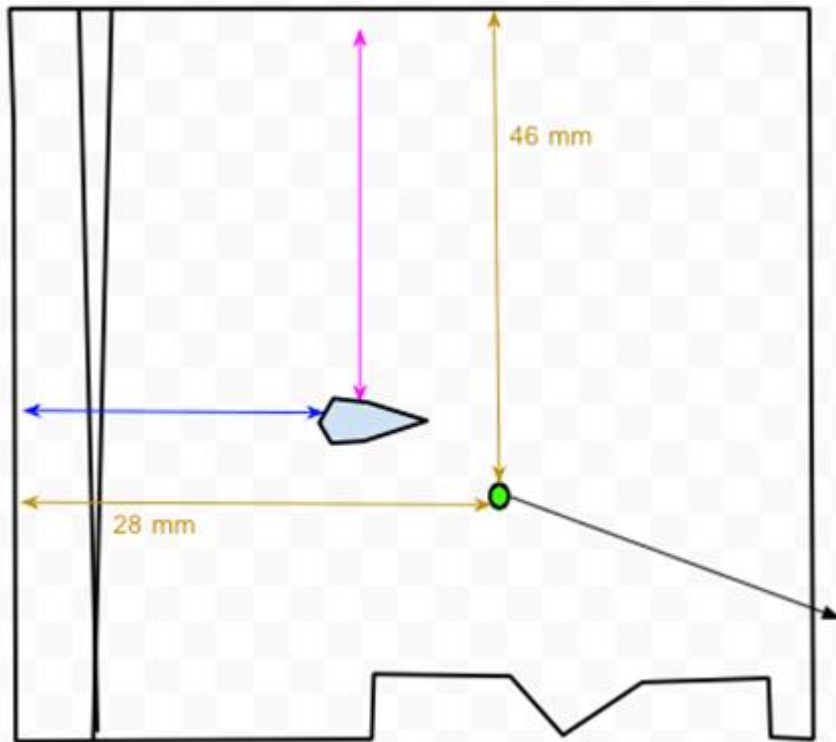


Figure 21: A scheme of location of green point laser on a luminescence plate for the second shot.

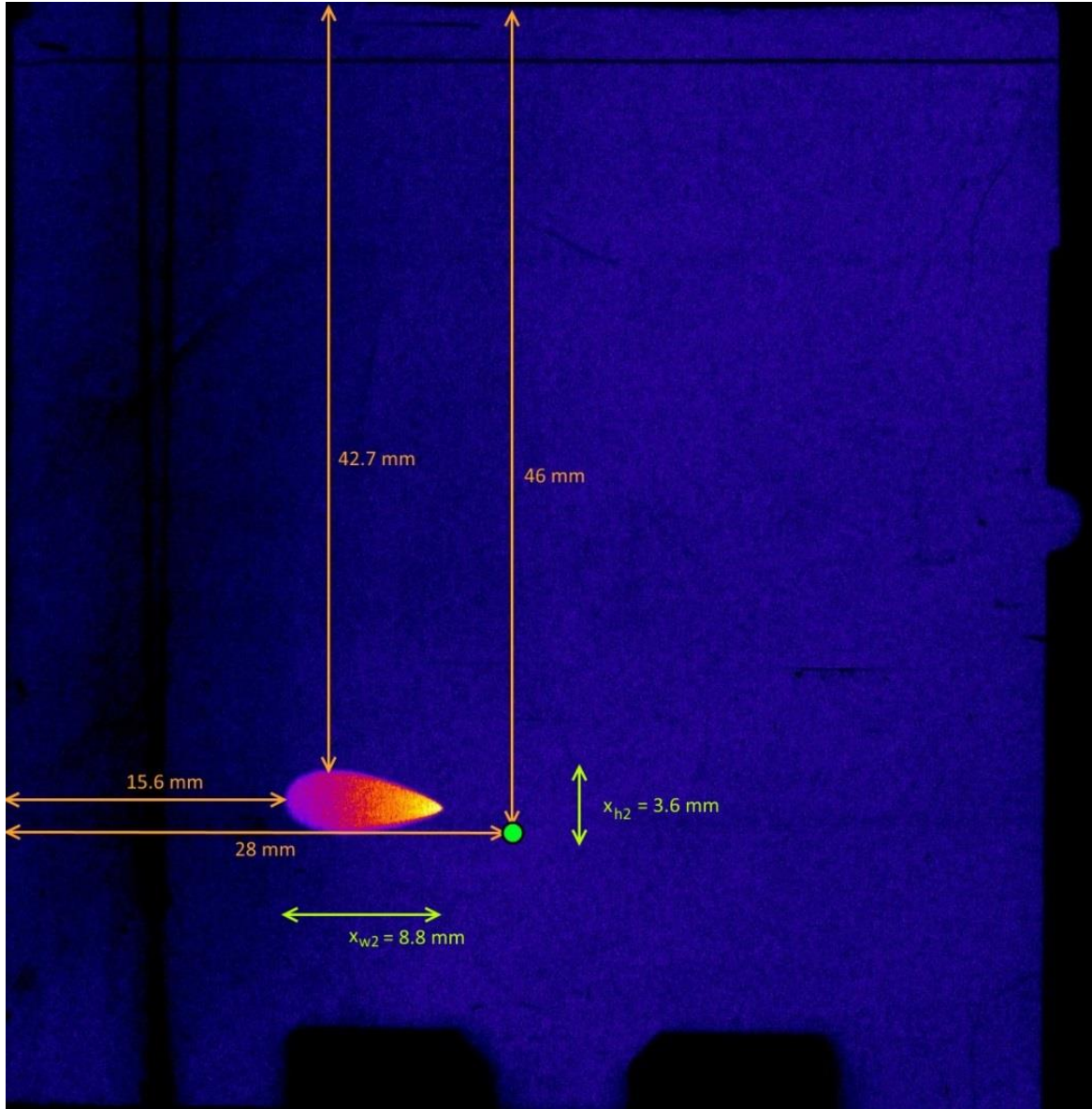


Figure 22: A picture of the luminescence plate with marked dimensions of the second shot.

4.4.2.1. Vertical direction

According to knowledge of trigonometric functions, we are able to calculate the output angle and divergence in vertical directions. In Figure 22, measured distances of the beam spots and its dimension from the edges are shown and in Figure 23 is schematic picture of location.

$$x_{ver2} = 46 \text{ mm} - 42.7 \text{ mm} = 3.3 \text{ mm}$$

The output angle in vertical direction we calculated as previously. The opposite is equal to the value x_{ver2} and the adjacent is equal to a distance between the imaging plate

and the final collimator, which was $l_{IP2} = 41.9$ cm. Substituting in the correct units we obtain an angle θ_2 , which is the deflection in vertical direction.

$$\tan \theta_2 = \frac{x_{ver2}}{419} = \frac{3.3}{419}$$

$$\theta_2 = 0.45^\circ = 0^\circ 27'$$

Next, we obtained, from the measured proton beam height $x_{h2} = 3.6$ mm the divergence δ_2 in vertical direction. For example we can use the law of sines:

$$\frac{x_{h2}}{\sin \delta_2} = \frac{\sqrt{(x_{h2} - x_{ver2})^2 + l_{IP2}^2}}{\sin(90^\circ - \theta_2)}$$

$$\frac{3.6}{\sin \delta_2} = \frac{\sqrt{(3.6 - 3.3)^2 + 419^2}}{\sin(90^\circ - 0.45^\circ)}$$

$$\delta_2 = 0.49^\circ = 0^\circ 29'$$

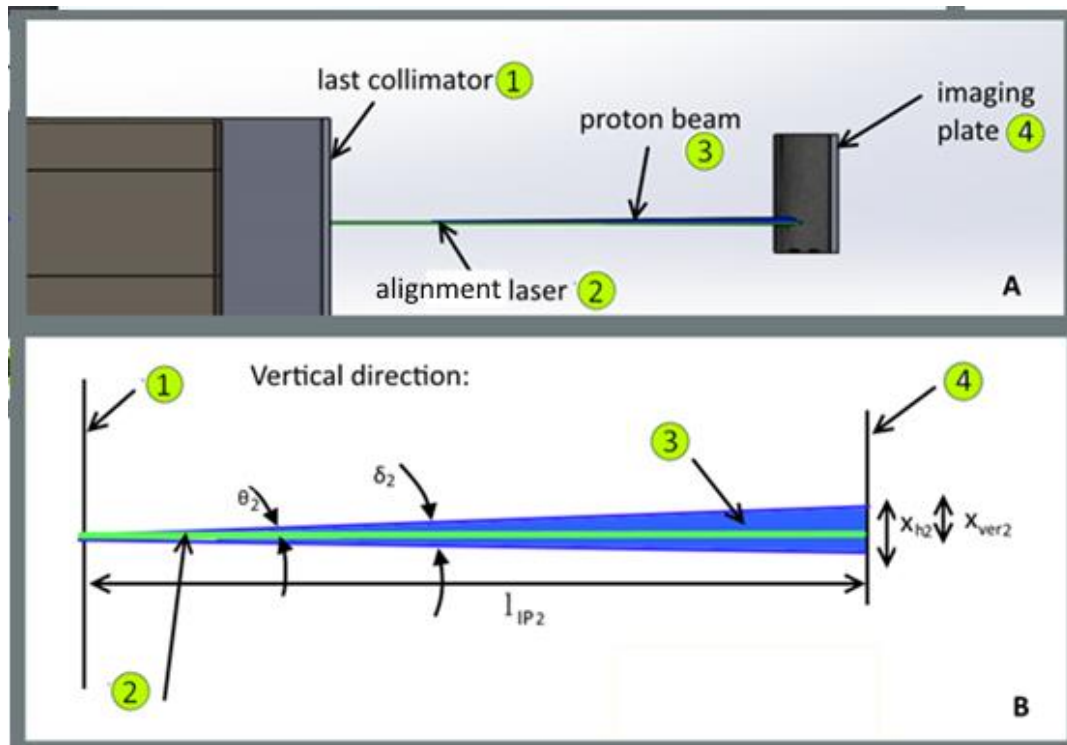


Figure 23: A) side view of the ESS output with visualised data from Imaging plate for detector, shot #2, B) The scheme of the vertical deflection proton beam from the alignment laser. (1-final collimator, 2- alignment laser, 3- proton beam, 4- imaging plate, l_{IP2} – distance from last collimator to imaging plate, x_{h2} – height of the proton beam, x_{ver2} – vertical displacement of proton beam, θ_2 – angle between alignment laser and proton beam, δ_2 – divergence of proton beam).

4.4.2.2. Horizontal direction

In Figure 22 are shown measured distances and in Figure 24 is schematic picture of location.

$$x_{hor2} = 28 \text{ mm} - 15.6 \text{ mm} = 12.4 \text{ mm}$$

The output angle in horizontal direction is the same as in previous part. Opposite is equal to the value x_{hor2} and adjacent is equal to a distance between the imaging plate and the final collimator, which is $l_{IP2} = 41.9 \text{ cm}$. Substituting in the correct units we obtained an angle φ_2 , which is a deflection in horizontal direction.

$$\tan \varphi_2 = \frac{x_{hor2}}{419} = \frac{12.4}{419}$$
$$\varphi_2 = 1.70^\circ = 1^\circ 41'$$

Next, we are able from the measured proton beam width $x_{w2} = 8.8 \text{ mm}$ obtain divergence ψ_2 in horizontal direction.

$$\frac{x_{w2}}{\sin \psi_2} = \frac{\sqrt{(x_{hor2} - x_{w2})^2 + l_{IP2}^2}}{\sin(90^\circ - \varphi_2)}$$
$$\frac{8.8}{\sin \psi_2} = \frac{\sqrt{(12.4 - 8.8)^2 + 419^2}}{\sin(90^\circ - 1.7^\circ)}$$
$$\psi_2 = 1.20^\circ = 1^\circ 12'$$

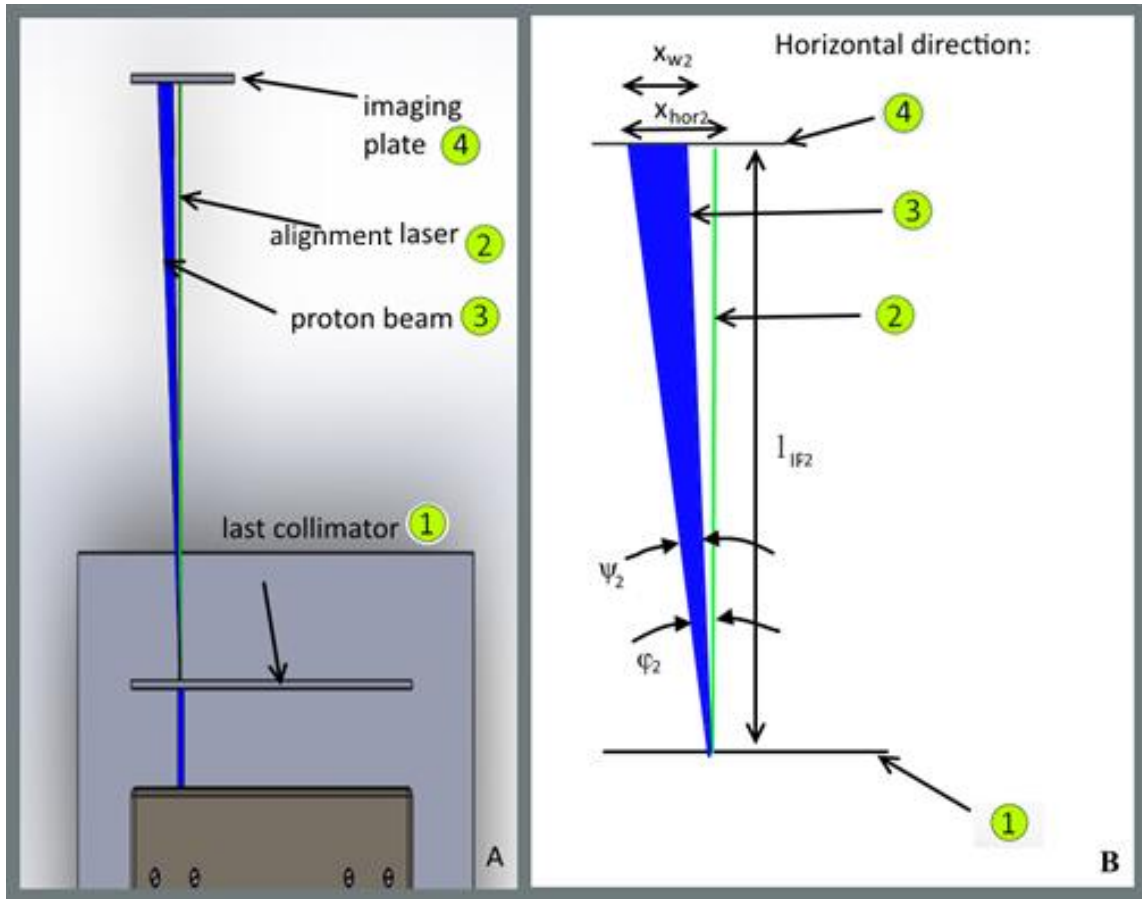


Figure 24: A) Top view of the ESS output with visualised data from Imaging plate for detector, shot #2 B) The scheme of the horizontal deflection proton beam from trace laser (1-final collimator, 2- alignment laser, 3- proton beam, 4- imaging plate, l_{IP2} – distance from last collimator to imaging plate, x_{w2} – width of the proton beam, x_{hor2} – horizontal displacement of proton beam, φ_2 – angle between proton beam and alignment laser, ψ_2 – divergence of proton beam)

5. Conclusion

The aim of this thesis was to characterize the geometry of laser-driven proton beam and the output angle due to the future potential of use in medical applications. An energy selector system has been realized for relatively low proton energies up to 60 MeV. As we can see in Figure 15 in chapter 4.2, the position of the selection slit is closer to the primary path for higher energies. The higher the energy considered, the smaller displacement of the selection slit is needed. However, due to the spatial mixing effect caused by the wide angular distribution of the laser driven proton beams currently available, the slit was not capable of isolating a specific value of energy, releasing protons with both higher and lower energy than needed.

For medical purposes it is desirable to apply the proton beam with the right energy (minimal energy distribution around the chosen value) due to the location of the Bragg peak. The calculation of the beam trajectory has been simplified for homogenous magnetic field and uses simple mathematic relations. The magnetic field was measured with a Hall probe along the path of the proton beam, which enters the Energy Selector System (ESS) 10 mm from the left aluminium collimator edge placed 25 mm upstream the first dipole. The profile of the magnetic field deviates from the ideally desired theoretical shape, adversely influencing the precision of the calculations and the experiment itself.

When the particles travel inside the first dipole, the magnetic field separates them according to their energy and the position of the selection slit can choose the required energy. But because there is a problem with the magnetic homogeneity, dipole may bend particles with different energy in the same position.

As we can see in Figure 18 and Figure 22 from experimental data, the proton beam spot has a droplet shape. This is caused by the spatial mixing effect and inhomogeneity of the magnetic field in region of the magnet, where we sent the proton beam. TNSA regime accelerates particles with all energies on interval from the lowest up to 60 MeV. Before particles enter the first dipole, there is a collimator, which selects a small part of the proton beam into a circular hole. Collimators used in the described experiments had a 3 mm diameter aperture. The aperture size influences the position of protons at the input to the

ESS, which could result in particles with different energies being bent into the slit position and mixed together. It can be partly solved by reducing the diameter of the collimator.

The output angle can be influenced by moving the last magnet forwards or backwards. Because of the inhomogeneous magnetic field and the spatial mixing effect, the beam, which leave's the ESS, has an irregular shape. Nonetheless, it is possible to measure the output angle in vertical and horizontal direction and calculate the divergence of the beam.

Two shots were taken to be compared with each other. They were made in different distances. The first shot was placed closer to the last collimator than the second one. The first shot has a significantly smaller output angle in horizontal direction, but larger output angle in vertical direction than the second shot. The divergence of the proton beam is smaller in vertical direction for the first shot, but in horizontal direction is smaller for the second shot. According to this perception it could be said, that the proton beam disperses vertically and focuses horizontally after leaving the last collimator.

Table 1: Summaries of angle results for two shots in vertical and horizontal direction

	Vertical		Horizontal	
	Output angle θ	Divergence δ	Output angle φ	Divergence ψ
Shot 1	0.65°	0.33°	1.45°	1.32°
Shot 2	0.45°	0.49°	1.70°	1.20°

As was mentioned in previous chapters, parameters of proton beam produced by TNSA regime cannot be perfectly replicated, because the arising plasma is always somewhat different. Energies that can be currently obtained with this regime, about 30-40 MeV as maximum cut-off are relatively low, for medical applications, for which at least 30 MeV is needed.

The ESS is still in a prototype state, the problem with spatial mixing effect will be solved using different collimation system and letting the beam pass through the homogenous magnetic field region. Indeed, during the experiment the measurement was partly improved by selecting a smaller diameter of collimator. Future experiments will be

set up with different parameters of collimators and the proton beam will enter the ESS in more homogenous part of magnetic field (in the middle of the dipole). As the position of entry will change, it is necessary to move the second and the third dipole so that the beam passes through the gap. Future assumption is that the output beam spot will have the fluence distribution more uniform and an elliptical shape, according to new simulation results.

References

- [1] DAIDO, Hiroyuki, Mamiko NISHIUCHI, Alexander S PIROZHKOV, Yoshiki NAKAI, Manabu TANOUE, Shuji KONDO, Shuhei KANAZAWA, Alexander PIROZHKOV, Timur ESIRKEPOV, Yukio HAYASHI, Koichi OGURA, Hideyuki KOTAKI, Masayuki SUZUKI, Izuru DAITO, Hajime OKADA, Atsushi KOSUGE, Yuji FUKUDA, Mamiko NISHIUCHI, Masaki KANDO, Sergei BULANOV, Keisuke NAGASHIMA, Mitsuru YAMAGIWA, Kiminori KONDO, Akira SUGIYAMA, Paul BOLTON, Shinichi MATSUOKA a Hirofumi KAN. Review of laser-driven ion sources and their applications. *Reports on Progress in Physics*. 2012-05-01, vol. 75, issue 5, s. 056401-. DOI: 10.1088/0034-4885/75/5/056401.
- [2] FOURKAL, E., J. S. LI, M. DING, T. TAJIMA a C.-M. MA. Particle selection for laser-accelerated proton therapy feasibility study. *Medical Physics*. 2003, vol. 30, issue 7, s. 1660-. DOI: 10.1118/1.1586268
- [3] LINZ, Ute a Jose ALONSO. What will it take for laser driven proton accelerators to be applied to tumor therapy?. *Physical Review Special Topics - Accelerators and Beams*. 2007, vol. 10, issue 9, s. -. DOI: 10.1103/PhysRevSTAB.10.094801
- [4] Vu Nguyen. Business. The New York Times Company. [online]. 17.5.2015 [ref. 2015-05-17]. Available from: http://www.nytimes.com/interactive/2007/12/14/business/20071217_PROTON_GRAPHIC.html?_r=0#step1
- [5] DE LANEY, Thomas F a Hanne M KOOY. *Proton and charged particle radiotherapy*. Philadelphia: Wolters Kluwer Health/Lippincott Williams, c2008, x, 274 p. ISBN 07-817-6552-8.
- [6] Zemen EM, Schreiber EC, Tepper JE. Basics of radiation therapy. In: Niederhuber JE, Armitage JO, Doroshow JH, et al., eds. *Abeloff's Clinical Oncology*. 5th ed. Philadelphia, PA: Elsevier Churchill Livingstone; 2013:chap 27.
- [7] AMALDI, Ugo a Gerhard KRAFT. Particle Accelerators Take up the Fight against Cancer. *CERN Courier*. 2006, Vol. 46, No. 10. Available from: <http://cerncourier.com/cws/article/cern/29777>
- [8] WIEDEMANN, Helmut. *Particle accelerator physics*. 3rd ed. Berlin: Springer, 2007. ISBN 978-354-0490-432.

- [9] PEACH, K, P WILSON a B JONES. Accelerator science in medical physics. *The British Journal of Radiology*. 2011, vol. 84, special_issue_1, S4-S10. DOI: 10.1259/bjr/16022594.
- [10] REICHL, Jaroslav a Martin VŠETIČKA. Encyklopedie fyziky [online]. 2006 - 2012 <http://fyzika.jreichl.com/> [ref. 2015-01-24]
- [11] [DR. PAUL PETER URONE, [Dr.California State University Sacramento. *College physics*. Houston, Texas: OpenStax College, Rice University, 2013. ISBN 978-193-8168-000.
- [12] Energy in Newtonian mechanics and in relativity. *UNSW Australia* [online]. Sydney [ref. 2015-04-30]. Available from: http://newt.phys.unsw.edu.au/einsteinlight/jw/module5_dynamics.htm
- [13] Giap H, Giap B. Historical perspective and evolution of charged particle beam therapy. *Transl Cancer Res* 2012;1(3):127-136. DOI: 10.3978/j.issn.2218-676X.2012.10.09
- [14] PLETTNER, Tomas, Robert L BYER a Robert H SIEMANN. The impact of Einstein's theory of special relativity on particle accelerators. *Journal of Physics B: Atomic, Molecular and Optical Physics*. 2005-05-14, vol. 38, issue 9, S741-S752. DOI: 10.1088/0953-4075/38/9/020.
- [15] HANNA, Samy. *RF linear accelerators for medical and industrial applications*. Boston: Artech House, c2012, xi, 202 p. Artech House microwave library. ISBN 16-080-7090-5.
- [16] NOLZ, Florian. *Wikipedia: the free encyclopedia* [online]. San Francisco (CA): Wikimedia Foundation, 2001-[ref. 2015-04-30]: http://commons.wikimedia.org/wiki/File:Wideroe_linac_en.svg
- [17] SCUDERI, V., S. BIJAN JIA, M. CARPINELLI, G.A.P. CIRRONE, G. CUTTONE, G. KORN, T. LICCIARDELLO, M. MAGGIORE, D. MARGARONE, P. PISCIOTTA, F. ROMANO, F. SCHILLACI, C. STANCAMPIANO a A. TRAMONTANA. Development of an energy selector system for laser-driven proton beam applications. *Nuclear Instruments and Methods in Physics Research Section A: Accelerators, Spectrometers, Detectors and Associated Equipment*. 2014, vol. 740, s. 87-93. DOI: 10.1016/j.nima.2013.10.037.

- [18] CIRRONE, Giuseppe A.P., Massimo CARPINELLI, Giacomo CUTTONE, Santo GAMMINO, S. BIJAN JIA, Georg KORN, Mario MAGGIORE, Lorenzo MANTI, Daniele MARGARONE, Jan PROKUPEK, Marcella RENIS, Francesco ROMANO, Francesco SCHILLACI, Barbara TOMASELLO, Lorenzo TORRISI, Antonella TRAMONTANA, Andriy VELYHAN, Mamiko NISHIUCHI, Masaki KANDO, Sergei BULANOV, Keisuke NAGASHIMA, Mitsuru YAMAGIWA, Kiminori KONDO, Akira SUGIYAMA, Paul BOLTON, Shinichi MATSUOKA a Hirofumi KAN. ELIMED, future hadrontherapy applications of laser-accelerated beams. *Nuclear Instruments and Methods in Physics Research Section A: Accelerators, Spectrometers, Detectors and Associated Equipment*. 2013, vol. 730, special_issue_1, s. 174-177. DOI: 10.1016/j.nima.2013.05.051.
- [19] Zeitoun, P.; Oliva, E.; Le, T.T.T.; Ros, D.; Sebban, S.; Li, L.; Velarde, P.; Fajardo, M. X-ray Chirped Pulse Amplification: towards GW Soft X-ray Lasers. *Appl. Sci.* 2013, 3, 581-592.
- [20] Pascal d'Oliveira. Dossier: Les lasers à l'IRAMIS. CEA. [online]. 21.5.2015 [ref. 2015-05-21]. Available from: <http://iramis.cea.fr/Comm/2010laserIRAMIS/AmplificateurImpulsion.jpg>
- [21] DZELZAINIS, T., G. NERSISYAN, D. RILEY, L. ROMAGNANI, H. AHMED, A. BIGONGIARI, M. BORGHESI, D. DORIA, B. DROMEY, M. MAKITA, S. WHITE, S. KAR, D. MARLOW, B. RAMAKRISHNA, G. SARRI, M. ZAKA-UL-ISLAM, M. ZEPF a C.L.S. LEWIS. The TARANIS laser: A multi-Terawatt system for laser-plasma investigations. *Laser and Particle Beams* [online]. 2010, vol. 28, issue 03, s. 451-461 [ref. 2015-05-07]. DOI: 10.1017/s0263034610000467.

- [22] PFOTENHAUER, S M, O JÄCKEL, A SACHTLEBEN, J POLZ, W ZIEGLER, H-P SCHLENVOIGT, K-U AMTHOR, M C KALUZA, K W D LEDINGHAM, R SAUERBREY, P GIBBON, A P L ROBINSON, H SCHWOERER a A. TRAMONTANA. Spectral shaping of laser generated proton beams. *New Journal of Physics*. 2008-03-01, vol. 10, issue 3, s. 033034-. DOI: 10.1088/1367-2630/10/3/033034.
- [23] KIRIYAMA, Hiromitsu, Takuya SHIMOMURA, Michiaki MORI, Yoshiki NAKAI, Manabu TANOUE, Shuji KONDO, Shuhei KANAZAWA, Alexander PIROZHKOV, Timur ESIRKEPOV, Yukio HAYASHI, Koichi OGURA, Hideyuki KOTAKI, Masayuki SUZUKI, Izuru DAITO, Hajime OKADA, Atsushi KOSUGE, Yuji FUKUDA, Mamiko NISHIUCHI, Masaki KANDO, Sergei BULANOV, Keisuke NAGASHIMA, Mitsuru YAMAGIWA, Kiminori KONDO, Akira SUGIYAMA, Paul BOLTON, Shinichi MATSUOKA a Hirofumi KAN. Ultra-Intense, High Spatio-Temporal Quality Petawatt-Class Laser System and Applications. *Applied Sciences*. 2013, vol. 3, issue 1, s. 214-250. DOI: 10.3390/app3010214.
- [24] BONNET, T., M. COMET, D. DENIS-PETIT, F. GOBET, F. HANNACHI, M. TARISIEN, M. VERSTEEGEN a M. M. ALEONARD. Response functions of Fuji imaging plates to monoenergetic protons in the energy range 0.6–3.2 MeV. *Review of Scientific Instruments* [online]. 2013, vol. 84, issue 1 [ref. 2015-04-30]. DOI: 10.1063/1.4775719.
- [25] MANČIĆ, A., J. FUCHS, P. ANTICI, S. A. GAILLARD a P. AUDEBERT. Absolute calibration of photostimulable image plate detectors used as (0.5–20 MeV) high-energy proton detectors. *Review of Scientific Instruments* [online]. 2008, vol. 79, issue 7 [ref. 2015-05-06]. DOI: 10.1063/1.2949388.
- [26] The TESLA Test Facility FEL team; SASE FEL at the TESLA Facility, Phase 2, TESLA-FEL-2002-01, 2002.